OPTICAL PYROMETRY FOR NONCONTACT TEMPERATURE MEASUREMENT

by

Sara E. Moneyhun

Thesis submitted to the Faculty of the

Virginia Polytechnic Institute and State University

in partial fulfillment of the requirements for the degree of

MASTER OF SCIENCE

in

Electrical Engineering

APPROVED:

Richard O. Claus

Dr. R. O. Claus, Chairman

Gary S. Brown

Dr. G. S. Brown

Dr. I. Jacobs

October, 1990

Blacksburg, Virginia

OPTICAL PYROMETRY FOR NONCONTACT TEMPERATURE MEASUREMENT

Sara E. Moneyhun

Dr. R. O. Claus, Chairman

Electrical Engineering

(ABSTRACT)

A noncontact two-color pyrometer, which uses an infrared (IR) transmitting rod and IR lenses to optically measure the temperature of a molten particle as it falls in an evacuated drop tube, has been designed and tested in the laboratory and in the field. The design uses a calcium fluoride (CaF_2) rod which transports optical energy radiated from the molten particle to a beam splitter, where it is split into two signals. Each signal is filtered and focused onto an indium antimonide (InSb) photodetector which is liquid nitrgen (LN_2) cooled. A ratio of the detectors' outputs indicates the temperature of the molten particle.

In the laboratory, a blackbody calibrator is used as a source, and a shutter with a speed of 4 ms is used to simulate the particle dropping by the optical sensing port. The pyrometer has been calibrated for a particle temperature range of 650°C - 1200°C.

ACKNOWLEDGEMENTS

I would like to thank my mother for all her love, guidance, and support. I wish to dedicate this work to the memory of my father, Bobby Jim Moneyhun, whose tremendous thirst for knowledge made an extraordinary impact on my life.

I wish to sincerely thank my advisor, Dr. R. O. Claus, for his continued support and guidance; both of which made my stay at Virginia Tech an extremely rewarding experience. I wish to thank Dr. G. Brown and Dr. I. Jacobs for their generous aid, valuable comments, and for serving on my graduate committee.

I wish to express my sincere thanks to Russ May for his assistance and patience during my research work. His knowledge and experience saw me through various impediments. I wish to gratefully acknowledge the folks down at Marshall Space Flight Center, Tom Rathz of the University of Alabama at Huntsville, et al. for their time and patience in allowing me to instrument the materials processing drop tube. Many thanks also go to fellow graduate students, research associates, and friends at the Fiber & Electro-Optics Research Center and Virginia Tech who have made my graduate years very enjoyable.

TABLE OF CONTENTS

1.0 INTRODUCTION

The main emphasis of this research has been the development of an instrument capable of measuring the temperature of a small (~5 mm diameter) metallic pellet in free fall. Such pellets are typical of experiments performed at NASA's Marshall Space Flight Center (MSFC) Drop Tube Facility in Huntsville, Alabama. The drop tube, as illustrated in Figure 1.1, is an evacuated, 105 m tall tube, 25.4 cm in diameter, which gives researchers a facility to perform materials processing experiments in a low-gravity environment [1]. When materials are processed in containerless and low-gravity environments, several types of phenomena which can affect the solidification process can be reduced to a very low level of contribution to the solidification process. The result is the development of unique materials which can have different properties such as higher transition temperature superconductors.

Typical drop tube experiments to study solidification and containerless processing start by heating a small sample of the material at the top of the tube by an electron-beam furnace or an electromagnetic levitation/RF induction heating furnace. After the sample becomes molten, it is dropped down the tube. As the sample falls for the 4.5 seconds of free fall, it cools and solidifies. The sample can be retrieved from a trap at the bottom of the tube, and materials analyses are performed on the sample.

It would be highly desirable to determine the temperature history of a sample as it drops down the tube. Currently, this is estimated analytically by applying the

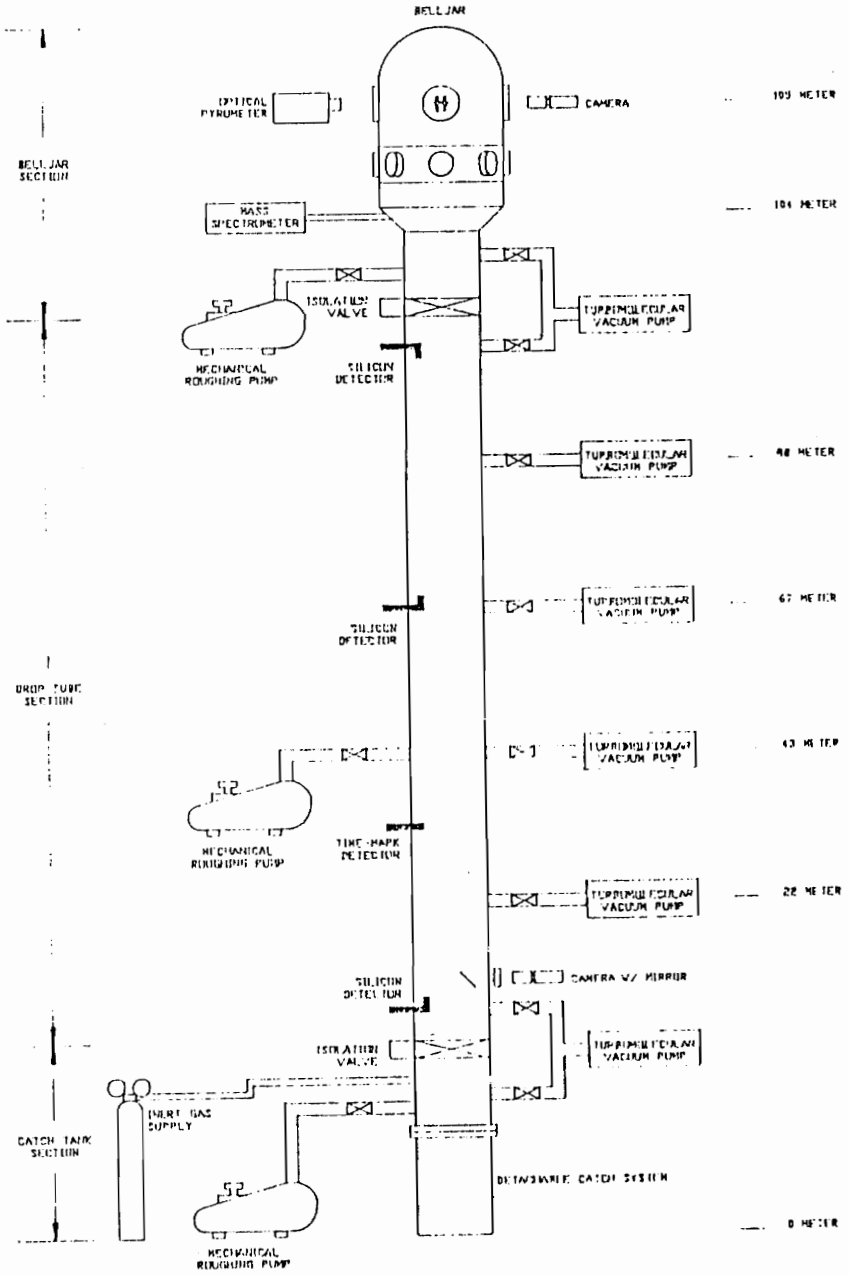

Figure 1.1. The figure shows a diagram of the 105 m tall drop tube at Marshall Space Flight Center in Huntsville, Alabama.

principles of thermal heat transfer to the known initial temperature of the sample and the elapsed time of the drop [2]. Some confidence in this analytically determined temperature history could be provided by measuring the temperature of the sample at one or more points along its drop with a noncontact temperature measurement system. Preliminary experiments toward this end were performed by Hoffmeister and Bayuzik [3]. Their approach utilized two-color pyrometry with silicon detectors, a fused silica lightpipe, and bandpass filters centered at 900 nm and 650 nm. The use of silicon detectors and the fused silica lightpipe effectively limits the measurement range of the instrument to a minimum temperature of about 1100°C, due to the transmission cutoff of silica above 2.0 μm. This deficiency would limit the use of this pyrometer to the beginning of the processing process where temperatures of the sample are above the cutoff temperature. The pyrometer developed in this research effort was intended to extend this temperature range down to 200°C by adopting indium antimonide detectors, calcium fluoride lenses and beam splitter, and a calcium fluoride lightpipe [4].

2.0 THEORY

In late 1900, a German physicist, Max Planck (1858 - 1947), formulated the radiation distribution law, known today as "Planck's Radiation Law." Experimental results at that time showed the new distribution law to be superior to all other existing distribution laws developed over a period of more than twenty years by Planck and some of his contemporaries, such as Wien, Kirchhoff, and Boltzmann, to name only a few. After the resolution of some minor experimental anomalies, it has continued to agree with observation ever since [5,6].

Every physical body above absolute zero in temperature emits spectral radiation which is dependent on its temperature. Planck's radiation law describes radiation of an ideal thermal radiator, a blackbody, and is given by

$$W_\lambda = \frac{C_1}{\lambda^5 \left[e^{C_2/(\lambda T)} - 1\right]} \quad [W/cm^2 \cdot \mu m], \tag{2.1}$$

where W_λ is the hemispherical spectral radiant energy, C_1 and C_2 are the radiation constants, whose presently accepted values are C_1=37,415 [$W \cdot \mu m^4/cm^2$], and C_2=14,388 [$\mu m \cdot K$], λ is the wavelength of radiation [μm], and T is the absolute temperature of blackbody [K] [7,8].

The radiation of a greybody, a real thermal radiator, deviates from blackbody radiation by a quantity called the hemispherical spectral emittance, $\epsilon_{\lambda,T}$, and is defined by [9]

$$\epsilon_{\lambda,T} = \frac{W_{\lambda a}}{W_{\lambda}} \cdot \tag{2.2}$$

The radiation and total power, respectively, from a greybody can be written as

$$W_{\lambda a} = \frac{C_1 \, \epsilon_{\lambda,T}}{\lambda^5 \, [e^{C_2/(\lambda T)} - 1]}, \tag{2.3}$$

and

$$W_{ta} = C_1 \int_0^{\infty} \frac{\epsilon_{\lambda,T}}{\lambda^5 \, [e^{C_2/(\lambda T)} - 1]} \, d\lambda. \tag{2.4}$$

Note that $\epsilon_{\lambda,T}$ varies with both λ and T, and is usually different for different materials. The ratio, or two-color, pyrometry technique requires that the radiant intensity, W_{λ}, be determined for two different wavelengths and then the ratio of the two W_{λ}s indicates a measure of temperature. The method can measure temperature relatively independent of variation in emissivity [10]. If the wavelengths are closely spaced so that the emissivity has not changed significantly, then the spectral emittance, ϵ_{λ}, can be approximated as a constant and will cancel from the ratio [7]. This can be shown numerically as

$$W_{\lambda 1} = \frac{\epsilon_{\lambda 1} \, C_1}{\lambda^5_1 \, [\, e^{C_2/\lambda_1 T} - 1 \,]} \tag{2.5}$$

$$W_{\lambda 2} = \frac{\epsilon_{\lambda 2} \, C_1}{\lambda^5_2 \, [\, e^{C_2/\lambda_2 T} - 1 \,]}, \tag{2.6}$$

and

$$\frac{W_{\lambda 1}}{W_{\lambda 2}} = \left(\frac{\lambda_2}{\lambda_1}\right)^5 \frac{\left[e^{(C_2/T\lambda_2)} - 1 \right]}{\left[e^{(C_2/T\lambda_1)} - 1 \right]} \tag{2.7}$$

where $\epsilon_{\lambda 1} = \epsilon_{\lambda 2}$.

3.0 MODEL FOR RATIO PYROMETER

Two sets of closely-spaced, infrared narrowband filters were selected to investigate ratio pyrometry experimentally. Narrowband filters were chosen to ensure that the emissivity does not change significantly within the wavelength region of interest. To take advantage of the temperature range of an IRCON blackbody calibrator (650°C - 1200°C) that was chosen as a source, the bandpass filters, obtained from CORION with specifications shown in Table 3.1, were chosen. A Fortran program (see Appendix A) was written using Planck's blackbody radiation equations to develop theoretical radiance curves for particular temperatures. Idealized spectral characteristics of the filters, which approximate the filters as a rectangular response, are shown graphically with respect to these theoretical radiance curves of the blackbody calibrator in Figure 3.1.

Another Fortran program was written to determine the theoretical radiant intensity available at the detectors after filtering (see Appendix B). The program incorporates a numerical integration subroutine which evaluates Planck's equation describing blackbody radiation over the idealized wavelength limits of each filter respectively as the temperature is varied from 500°C - 3500°C. A set of filter outputs, as a function of temperature, can be expressed as

$$F_1(T) = \int_{f_1-cut\ on}^{f_1-cut\ off} \frac{\epsilon_{\lambda,T}\, C_1}{\lambda^5 \left[e^{C_2/(\lambda T)} - 1\right]}\, d\lambda, \qquad (3.1)$$

and

	Center Wavelength (λ_o)	Full Width at Half Maximum (FWHM)	Transmittance
Filter Set A	1.991 μm	66.7 nm	55 %
	2.314 μm	80.5 nm	65 %
Filter Set B	2.823 μm	119 nm	69 %
	3.119 μm	107 nm	64 %

Table 3.1. Spectral filter specifications of narrowband filters obtained for pyrometry experiment.

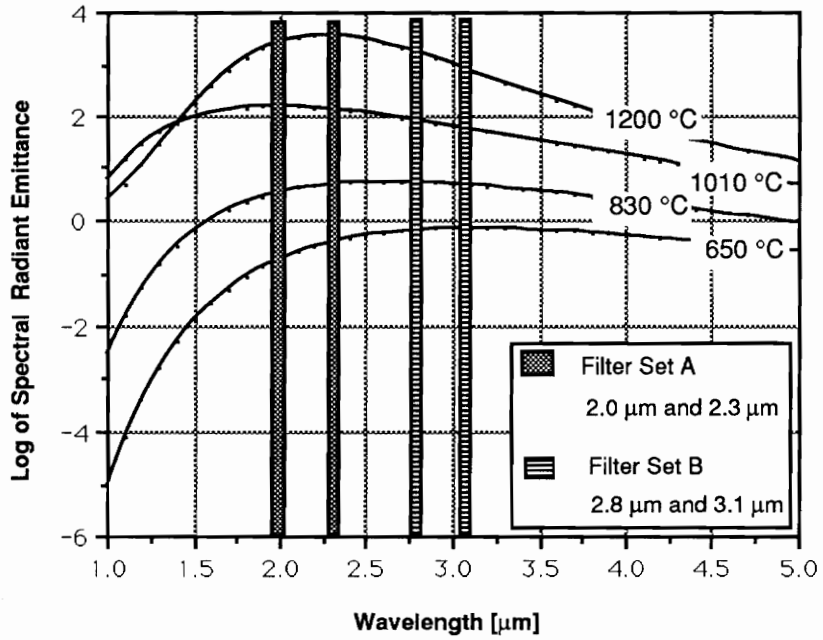

Figure 3.1. Graph of idealized spectral characteristics of two sets of narrowband infrared filters shown with respect to blackbody radiance curves.

$$F_2(T) = \int_{f_2-cut\ on}^{f_2-cut\ off} \frac{\epsilon_{\lambda,T}\, C_1}{\lambda^5\, [e^{C_2/(\lambda T)} - 1]}\, d\lambda. \qquad (3.2)$$

The program then calculates the ratio, $F_1(T)/F_2(T)$, at each temperature to obtain a single-valued curve which is a function of temperature and independent of source spectral emissivity. The theoretical models for both filter sets are shown in Figure 3.2 with the temperature axis limited to the range of the blackbody calibrator, 650°C - 1200°C. Exponential curves have been fit to the calculated results. The R^2 value associated with each regression equation to follow is called the coefficient of multiple determination. It is a criterion commonly used to illustrate the adequacy of a fitted regression model. The results of R^2 x 100% can be interpreted as the percentage variation of the data explained by the postulated model [11,12].

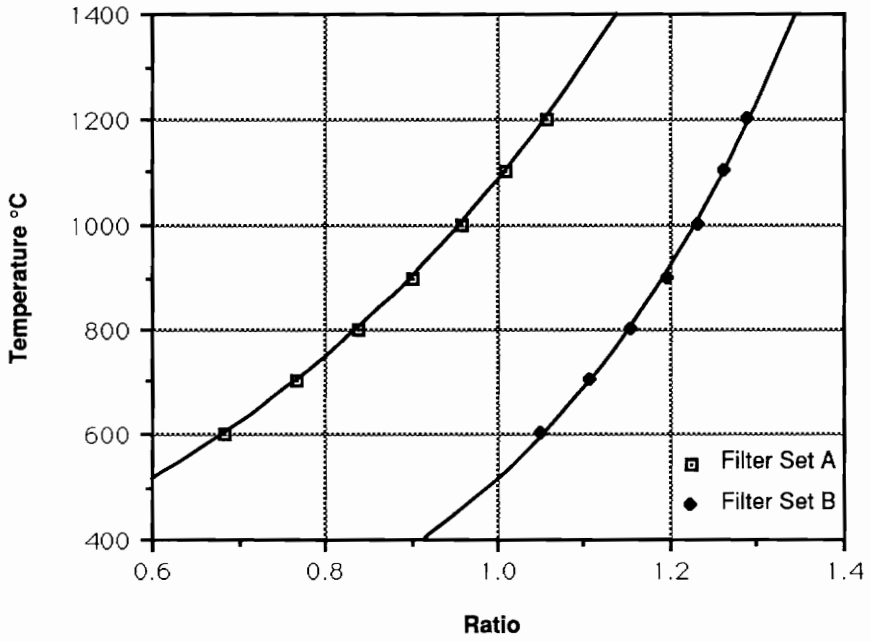

Exponential curve fit to Filter Set A

y = 168.23 * 10^(0.80775x) R^2 = 1.000

Exponential curve fit to Filter Set B

y = 27.581 * 10^(1.2677x) R^2 = 0.999

Figure 3.2. Graph shows the theoretical ratio of the energy at each temperature for both filter sets with exponential curves fit to the theoretical data.

4.0 EXPERIMENTS

4.1 Laboratory Component Experiments

4.1.1 Detector Linearity Tests

Two EG&G JUDSON Indium Antimonide (InSb) photodetectors were selected for use in the pyrometry experiments. The detectors, which are liquid nitrogen cooled, are responsive to light of wavelength 1 μm - 5.5 μm. Using calibrated neutral density filters, the linearity of both detectors was investigated. A neutral density filter is used to attenuate the intensity of incident light evenly over a broad spectral range.

The experimental set up is shown in Figure 4.1. The neutral density filters were placed as close to the detector as possible to ensure that the light entering the detector had been filtered. As in all the experiments to follow, the preamplifiers were biased with 12 V batteries and were properly grounded. The computer was equipped with an analog/digital converter, and a data acquisition software package was used to acquire the experimental data at a sampling rate of 50 Hz. With the blackbody calibrator radiating at 1200°C, the detector voltage was recorded for each neutral density filter. Both detectors were tested. With

$$\text{Loss} = 1 - 10^{-\text{O.D.}}, \tag{4.1}$$

where O.D. is the filter optical density, the results are shown in Figure 4.2. A curve is shown interpolated to the experimental data. The results illustrated in the figure show that both detectors behave nearly linear.

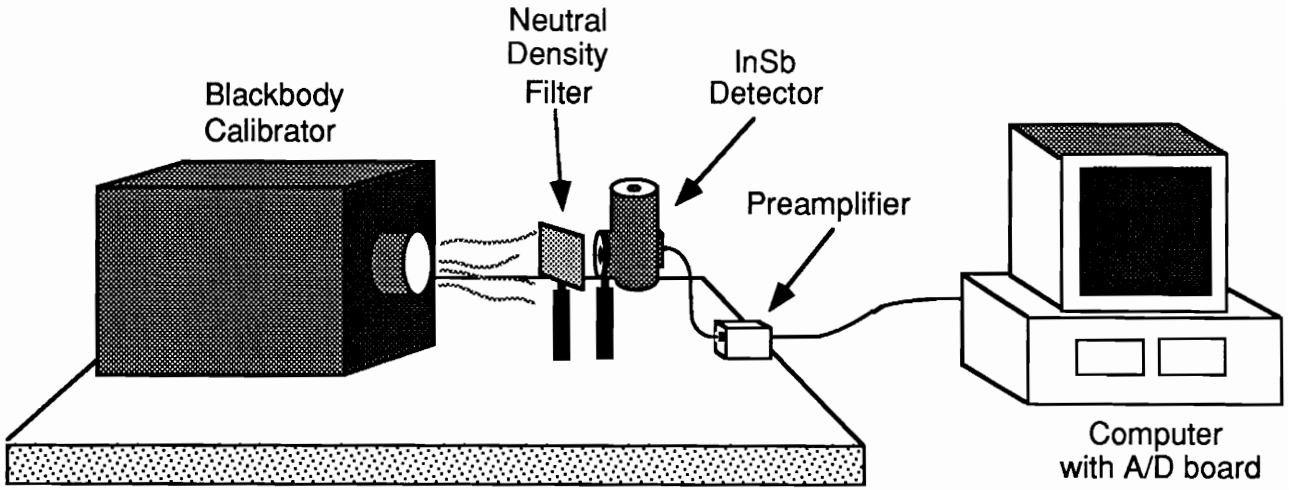

Figure 4.1. Picture of set up for testing linearity of both detectors.

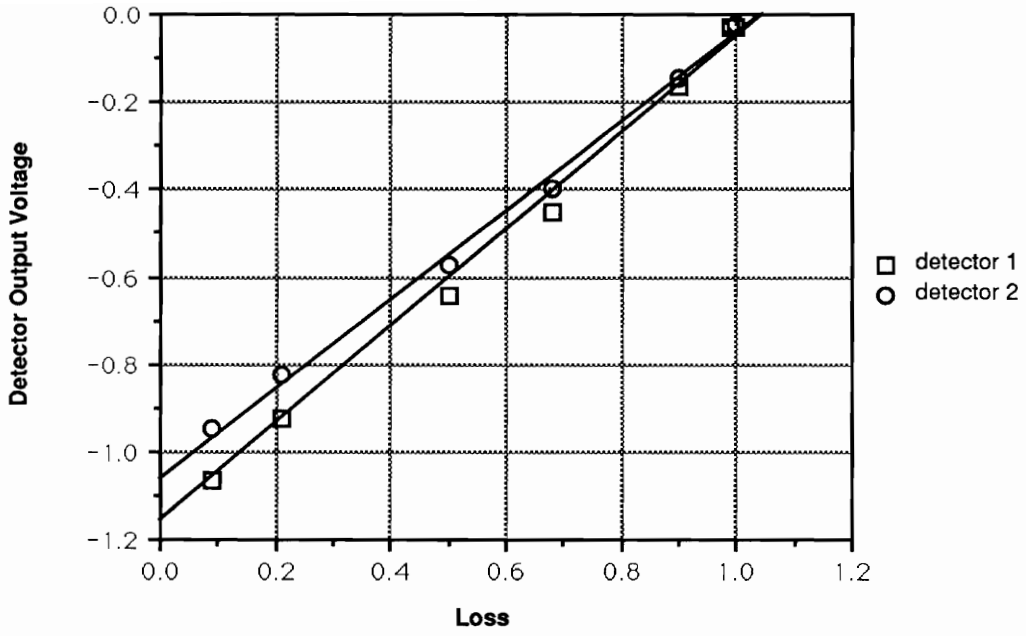

Figure 4.2. Graph of detector linearity for both detectors using calibrated neutral density filters to induce loss.

4.1.2 Filter Tests

In order to determine if the two sets of filters selected for the pyrometry experiment would yield the single-valued curves that were theoretically predicted in Figure 3.2, a simple experiment was performed. The experimental set up is shown in Figure 4.3. A metal pocket, not obstructing the detector's field-of-view, was mounted to each detector holder so that the filters were placed directly on the face of the detector. The pocket also allowed for ease in placement of the filters to be tested. As the temperature of the blackbody calibrator was varied from 650°C - 1200°C at increments of 50°C, detector voltage values were recorded for both sets of narrowband filters. The results for the ratio of the detector voltages at particular temperatures for both sets of filters are shown in Figures 4.4 and 4.5, respectively. An exponential curve is shown interpolated to the second set of experimental data.

Comparing the experimentally obtained graphs, which are shown in Figures 4.4 and 4.5, to the theoretical models for both filter sets of Figure 3.2, there is a drastic discrepancy between the model and the experimental data for the first filter set. It was believed that this problem was due to leakage of light away from the passband of the filter(s). Further investigation of the filter sets on a spectrum analyzer [FOA 2000] revealed that the sideband rejection of both filters in the first set was not sufficient to cover the wide bandwidth of the photodetector which is from 1 μm to 5.5 μm. For that reason, only the second filter set was used for the rest of the experiments and incorporated into the pyrometer. The model and the experimental data for the second filter set were in good agreement, with differences probably due to the transmittance of the filters, which was not

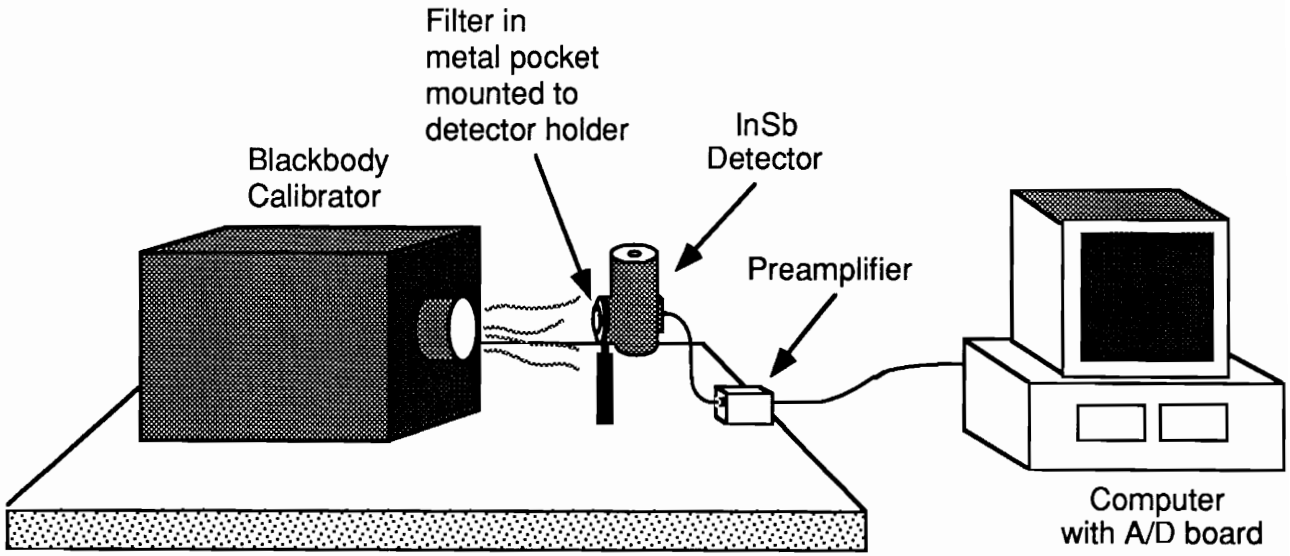

Figure 4.3. Picture of set up for testing both sets of narrowband infrared filters. The narrowband filters are placed in pocket to hold them directly up to detector face.

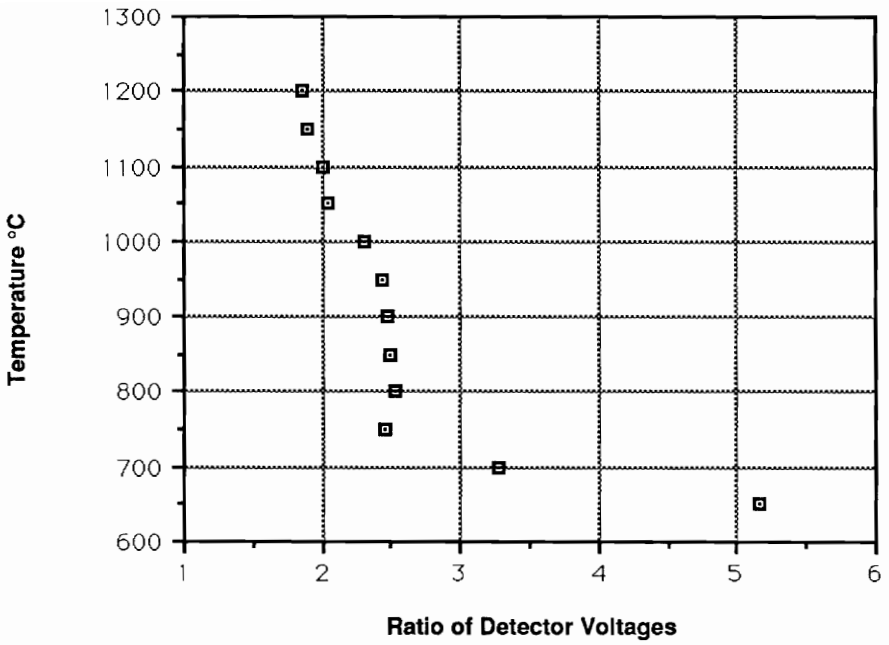

Figure 4.4. Graph of the ratio of the detector voltages at particular temperatures for Filter Set A (2.0 μm and 2.8 μm narrowband filters).

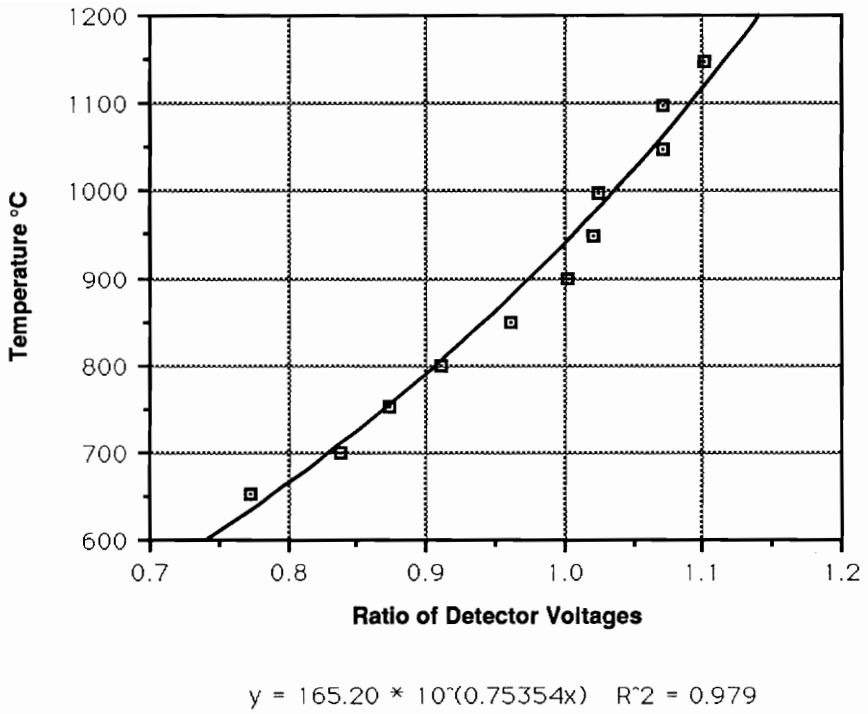

Figure 4.5. Graph of the ratio of the detector voltages at particular temperatures for Filter Set B (2.8 μm and 3.1 μm narrowband filters).

accounted for in the theoretical model.

4.1.3 Fiber Tests

In order to determine if enough power is present at the detector when using fibers to guide the infrared radiation, the experiment illustrated in Figure 4.6 was performed. First, a single zirconium fluoride fiber, one meter long, was investigated. Due to the small core diameter (200 μm) and high losses in the test grade fiber, insufficient power was intercepted from the blackbody calibrator, and power delivered to the detector was below the noise floor of the detector. Because of the expense and limited availability of experimental IR fibers such as zirconium fluoride, experiments with IR fiber bundles were impractical. For this reason, a circular bundle of hollow core optical fibers, drawn at Virginia Tech's Fiber & Electro·Optics facility, was investigated.

Recently, studies involving hollow core fibers and tubes have shown their ability to guide IR radiation [13-15]. Hollow core fibers, which use air as the radiation transmission medium, guide radiation by a different mechanism than step index fibers, which rely on a sequence of total internal reflections at the core-cladding interface. In hollow core fibers, only rays with a very small angle of incidence to the air-wall interface will be significantly reflected back towards the center of the fiber and consequently guided. Due to this manner of light guiding, one of the most serious problems in hollow core waveguides is high loss due to bending.

Two bundles of hollow core tubes were investigated experimentally. One of the fiber bundles investigated consisted of 35 fibers developed and manufactured at

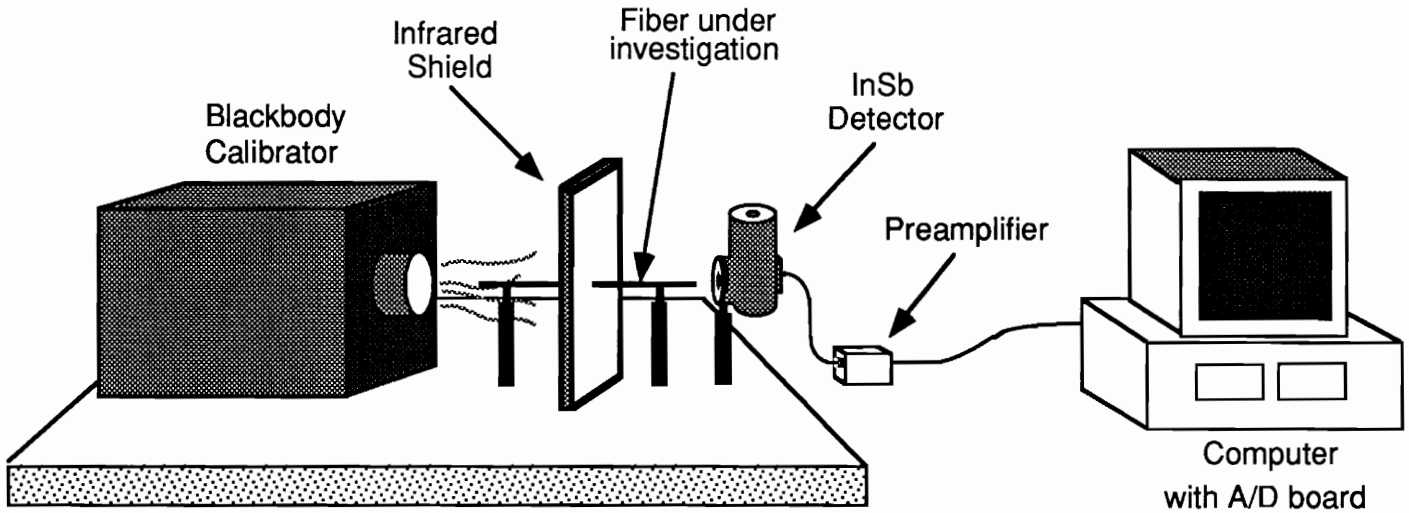

Figure 4.6. Picture of set up for testing various infrared guiding fibers.

Virginia Tech. They were all 30.48 cm long, and had inner core diameters of 245 μm. The second bundle, manufactured by Hughes Aircraft Company, consisted of 3 glass tubes, 30.48 cm long, with inner core diameters of 42 mm. The total outer diameter of both glass bundles was approximately 5.6 mm. The fibers were held straight and a shield was placed in front of the InSb detector to insure that only the light which passed through the fiber bundle arrived at the detector. The detector voltage was recorded as the temperature of the blackbody source was varied from 650°C - 1200°C at 50°C increments. The results are shown in Figure 4.7.

The results obtained from the experiment follow theory. Experimentally, we observe more power being guided through the fiber bundles as the temperature of the source is increased. We also see that larger inner core fibers transmit more power. Although more power was transmitted, it was not enough when used in conjunction with the infrared narrowband filters. The option of larger bundles of hollow core fibers was considered, but problems at the drop tube were foreseen. Because of the hollow nature of the fibers, evacuating the drop tube would become a problem if the bundle was to extend into the tube. A calcium fluoride window would need to be vacuum-fitted in the flange of the tube to prevent outgasing. The hollow core fibers would then view the molten particle through this substrate. In an attempt to ensure larger detected power levels and ease the complexity of instrumenting the drop tube, a standard diameter IR rod, which would use common vacuum-fittings to couple with the tube, was selected. A calcium fluoride rod, 2.54 cm in diameter and 15.24 cm in length, was obtained and tested in the laboratory. The results were promising, and the rod was incorporated as

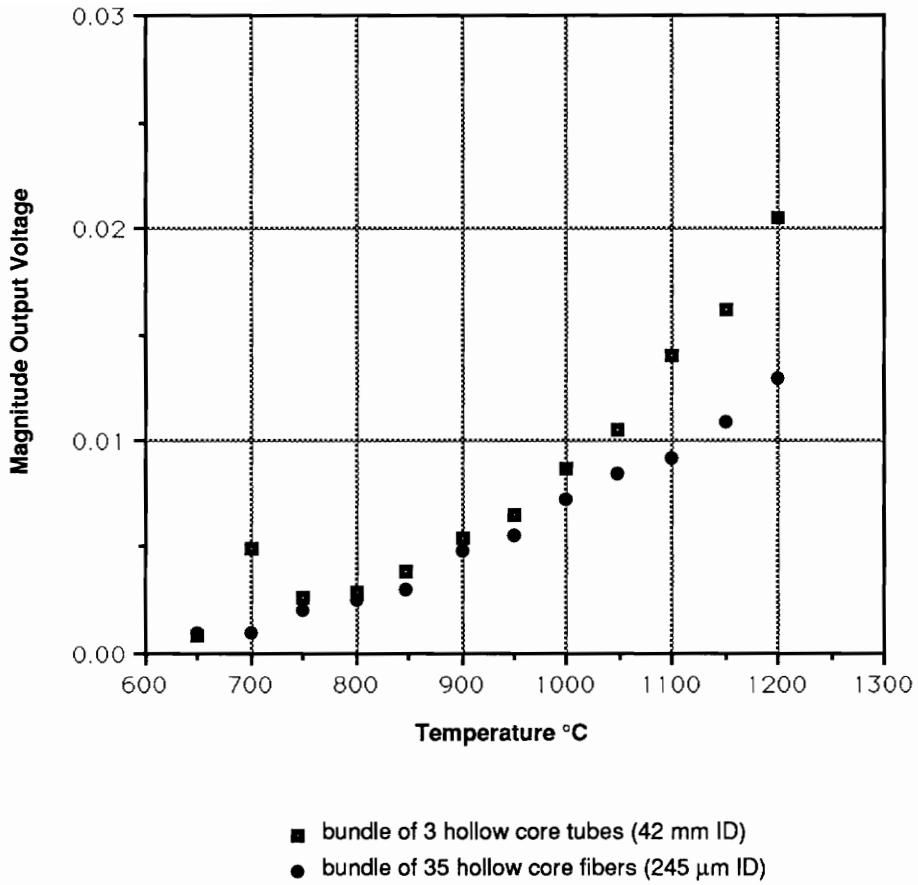

Figure 4.7. Graph of comparison of detector voltage magnitudes with respect to two different infrared fiber bundles.

the light guide into the pyrometry set up.

4.2 Prototype Pyrometer Design

4.2.1 Physical Set Up

A portable box with removable lid was constructed in order that the pyrometer could be mounted on the drop tube at Marshall Space Flight Center (MSFC) in Huntsville, Alabama. Figure 4.8 is a top view of component location in the prototype box. A detailed list of components used is given in Appendix C. The components were mounted on rails and x-y-z translators for ease of alignment.

4.2.2 Prototype Pyrometer Testing

In order to determine the temperature of a molten object within the pyrometer's field-of-view, an experiment was run to establish a calibration curve. The experiment was run several time in order to examine the repeatability of the measurement. The set up for the laboratory experiment is shown in Figure 4.9. The actual blackbody aperture on the calibrator was located 17.78 cm behind the front panel. The blackbody calibrator was placed 15.24 cm away from the end of the rod because of the intense heat which was radiated from the blackbody calibrator. A metal sheet with a variable speed shutter and variable iris mounted to it was placed between the pyrometer and the blackbody to ensure that the calcium fluoride rod did not sustain any thermal damage from prolonged exposure to the high temperatures of the blackbody calibrator.

The InSb detectors were cooled with liquid nitrogen for two hours before beginning the experiment to ensure minimal drift of the detector offset voltage. With the blackbody calibrator set at 650°C and the shutter open, the heights and

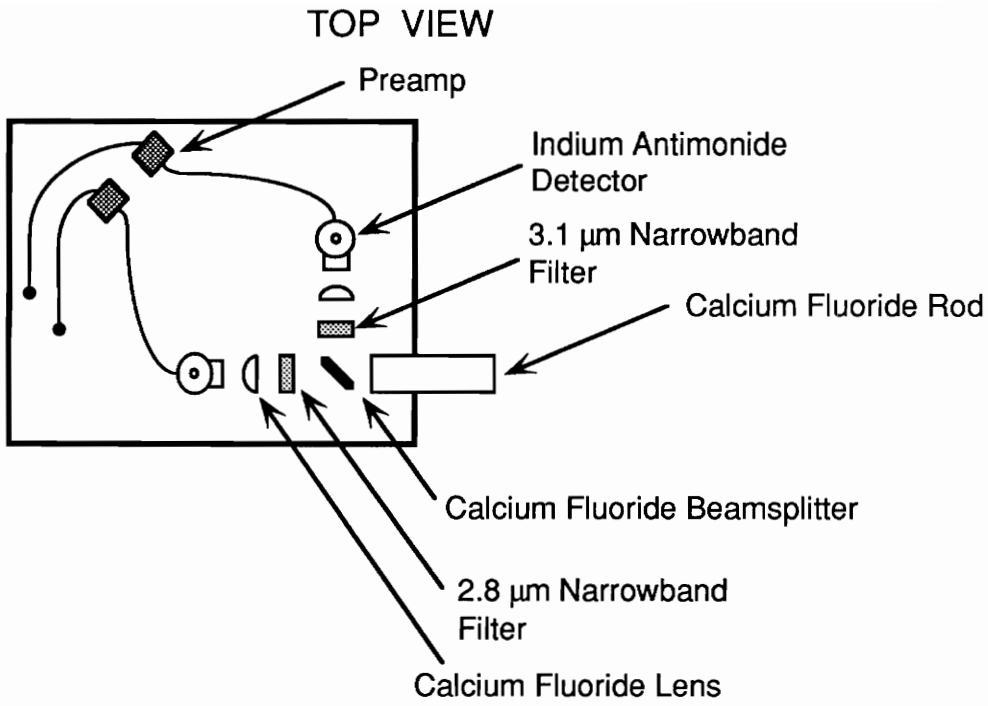

Figure 4.8. Picture of top view of component location in the prototype pyrometer box.

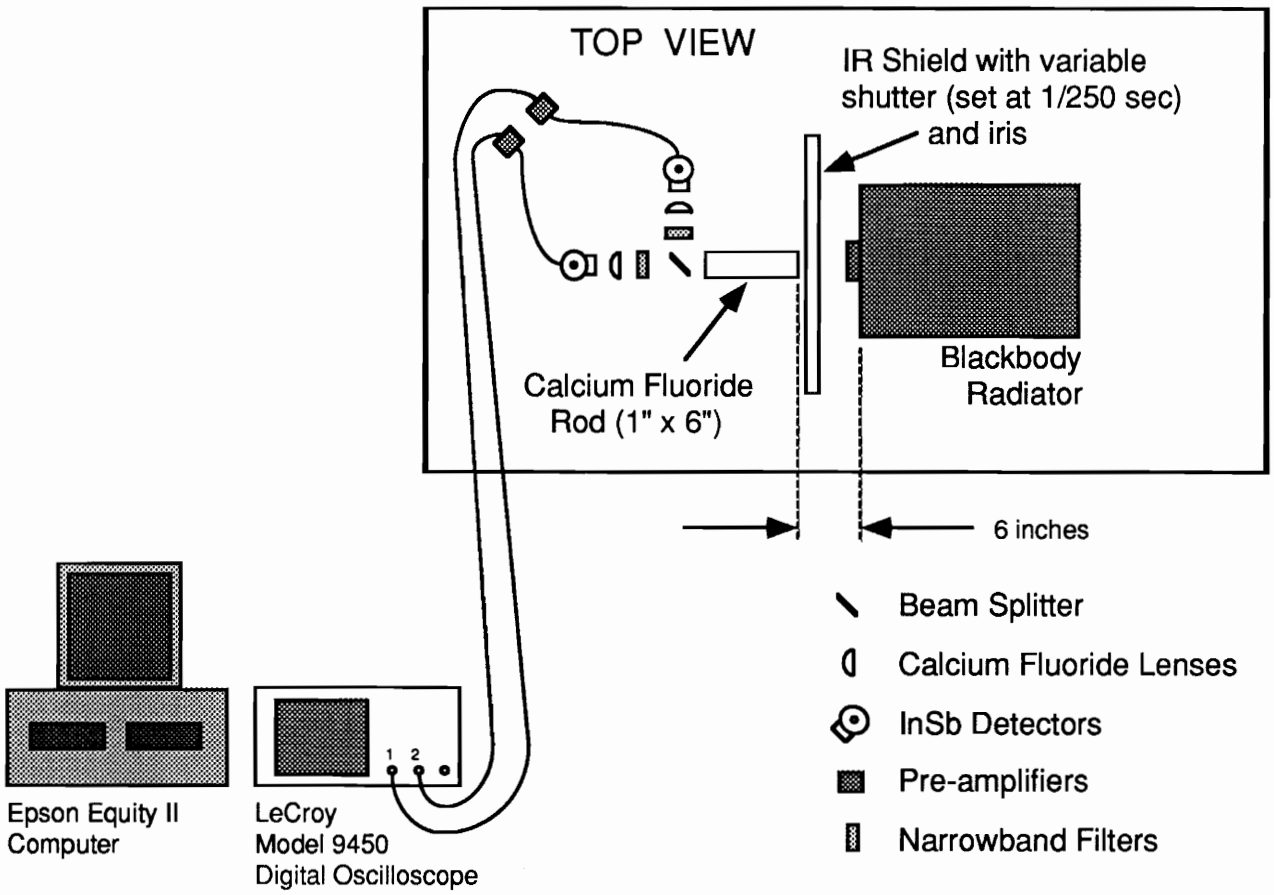

Figure 4.9. Picture of the laboratory set up used to test prototype pyrometer.

distances of all the components, as well as the angle of the beam splitter, were adjusted to allow for a maximum signal in both channels of the LeCroy digital oscilloscope. For each data point, the shutter was opened for 4 ms, to simulate a molten particle dropping by the pyrometer. As the temperature of the blackbody calibrator was increased from 650°C to 1200°C at 50°C increments, the magnitude of the change in detector voltage was determined at each 50°C increment in temperature. The change in detector voltage was determined by subtracting the initial offset voltage from the recorded detector magnitude for each channel at different temperatures. The initial detector offset voltage, which is due to dark current in the detectors, was also recorded. The ratio of the change in detector voltage for each channel was then taken and plotted with respect to the corresponding temperature. The test was repeated three times on different occasions, where all components were broken down and set up for each experiment. The resulting calibration curves are shown in Figure 4.10. The theoretical curve is shown along with the calibration curves. The differences between the various experimental runs is most likely due to component alignment in the pyrometer box. The results indicate that a calibration curve needs to be established each time the pyrometer is set up.

4.2.3 Test of Effects of Iris Diameter

The set up shown in Figure 4.11 was used to determine how the size of the molten particle to be evaluated will effect the performance of the pyrometer. A calcium fluoride beam splitter was used to split the light from the rod into two signals. Each narrowband filter was mounted together with a calcium fluoride lens which focused the light onto the detectors. A digital processing oscilloscope was used in

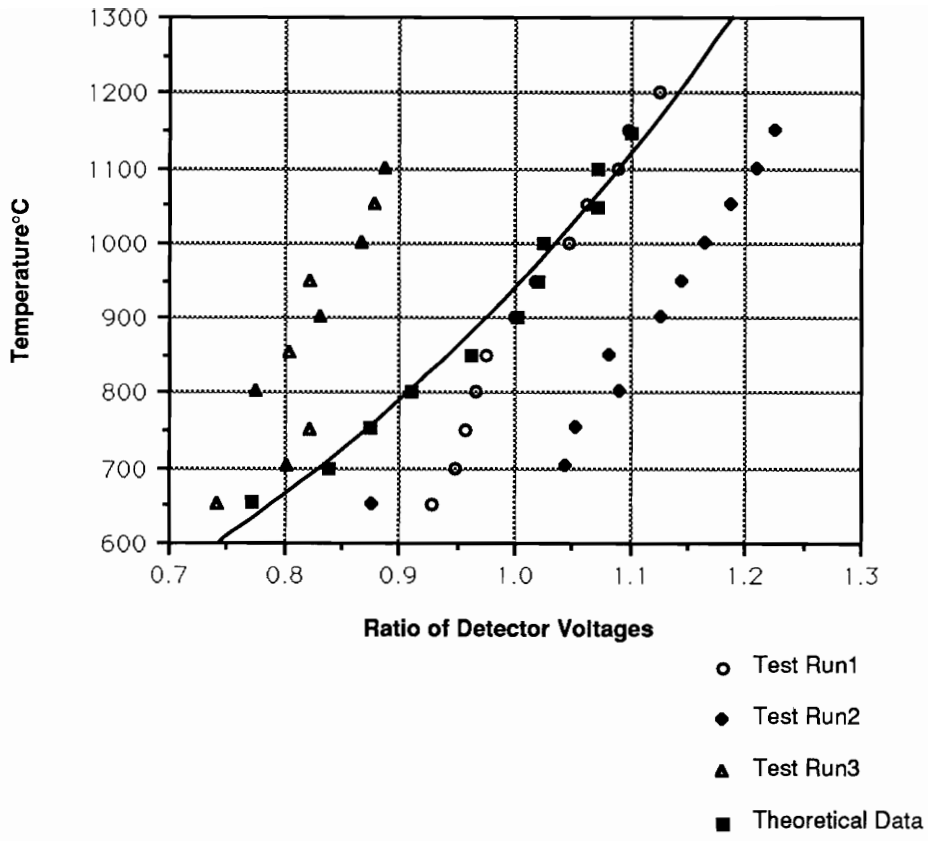

Figure 4.10. Graph of calibration curves obtained from three experimental tests of the prototype pyrometer.

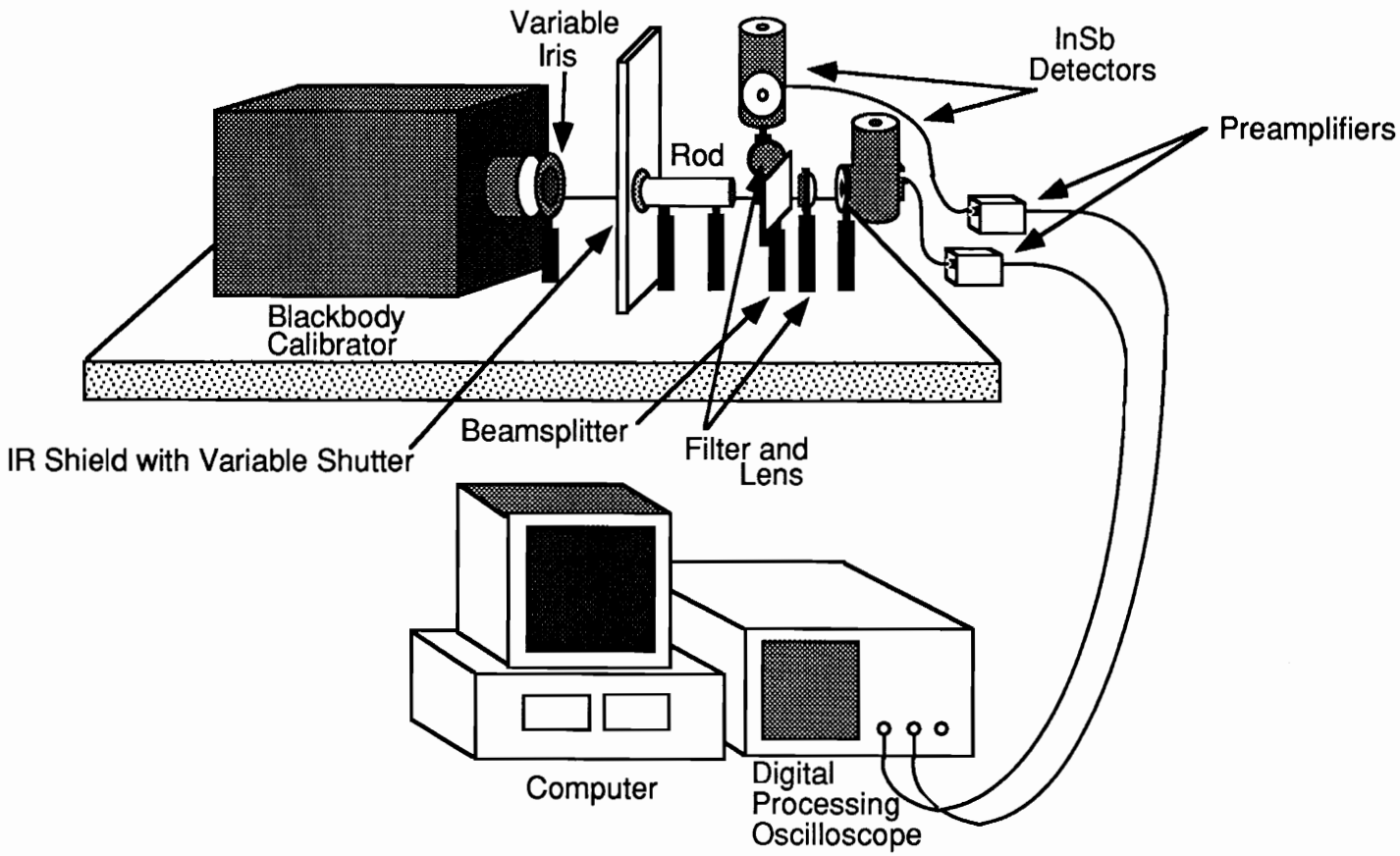

Figure 4.11. Picture of experimental set up for testing effects of iris diameter.

place of the A/D board to speed up the acquisition rate of the data. The oscilloscope was set to trigger on a positive slope and was acquiring at a rate of 10 kHz. The data was translated to the computer via a general purpose interface bus (GPIB). The blackbody radiator was set at 1000°C. The diameter of the iris, measured by digital calipers, was varied from 2 mm to 13 mm in increments of 1 mm. The shutter was opened for 4 ms, and the change in detector voltage was then determined. The results are shown in Figure 4.12. A plot of the signal-to-noise ratio (SNR) is shown in Figure 4.13.

Because a variable iris 17.78 cm in front of the blackbody aperture does not equivalently model a small radiating particle, the results do not necessarily give a limitation on the size of the particle. The results do show, however, that as the size of the iris decreases, the power intercepted by the pyrometer is insufficient. Even when the iris opening was 7 mm or more, the signal could barely be distinguished from the noise level of the detectors, and this caused the variations in the ratio data of Figure 4.12. This data indicates there may be power level problems because of small particle sizes when testing the pyrometer at the drop tube.

4.2.4 Angular Dependence Experiment

The set up shown in Figure 4.9 was used in order to test if the position of the molten particle falling down the drop tube will have an effect on pyrometer performance. The pyrometer box was moved linearly in a transverse direction to the blackbody calibrator. The box was moved in 12.5 mm increments for 6.35 cm to the right and left of the blackbody calibrator. The test was run for blackbody

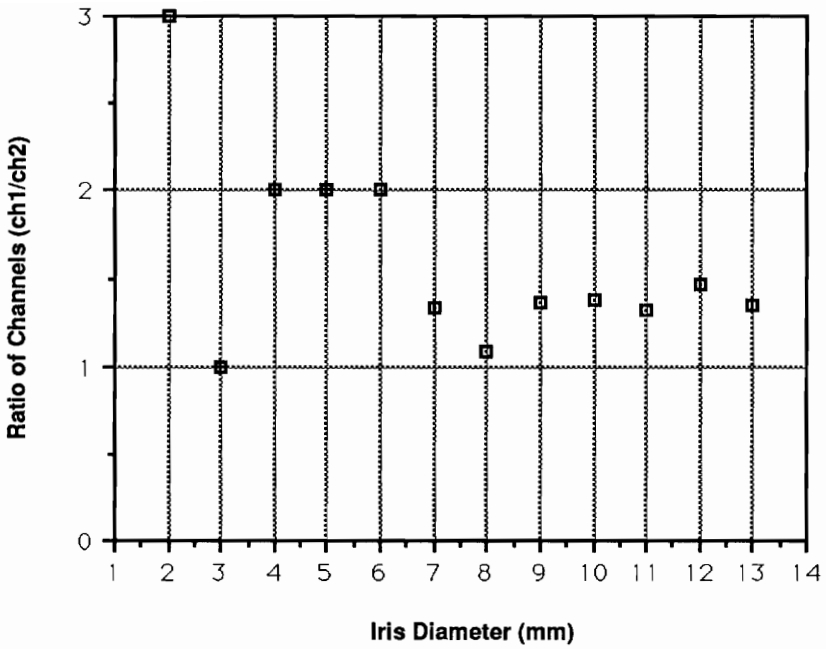

Figure 4.12. Graph of the change in the ratio of the detector outputs with respect to variations in iris diameter.

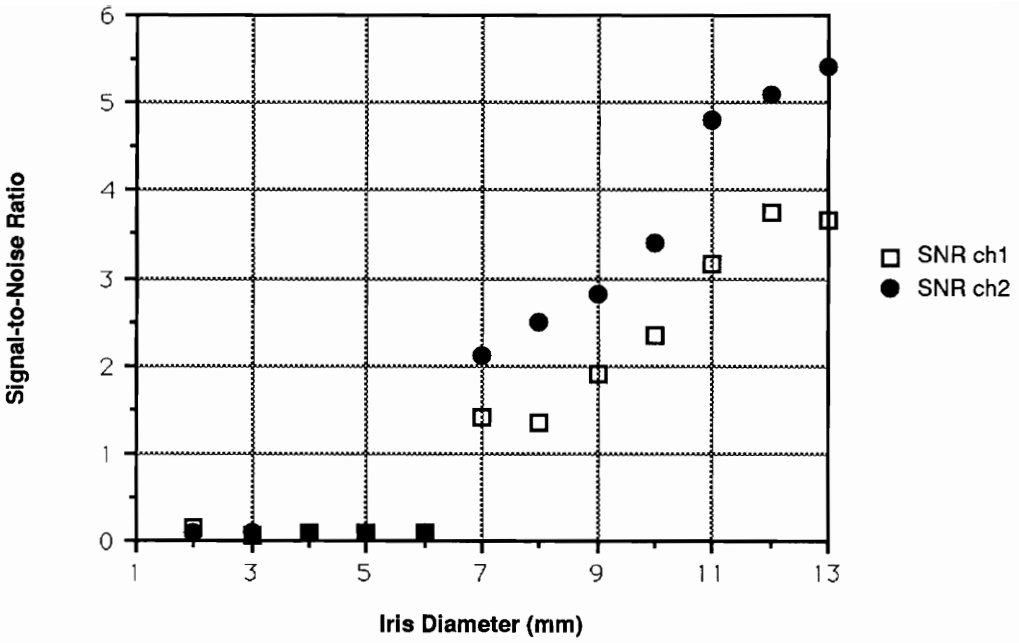

Figure 4.13. Graph of the signal-to-noise ratio for both detectors with respect to variations in iris diameter.

temperatures of both 1000°C and 1100°C. The change in detector voltages as a function of box position is shown in Figures 4.14 and 4.16, where the temperature of the calibration is 1000°C and 1100°C respectively. Figures 4.15 and 4.17 show the variation of the ratio of the detector voltages with respect to position for both 1000°C and 1100°C.

The data show that there will be a significant change in the ratio of the detector outputs with respect to the position of the particle. This may lead to serious problems in the effectiveness of the pyrometer when the position of the particle can not be controlled, such as in the drop tube application.

4.3 Field Tests of Prototype Pyrometer at NASA MSFC

While at Marshall Space Flight Center, niobium drops were used during the testing of the pyrometer. At the top of the drop tube, a niobium wire (62 mil diameter, MARZ grade) was fed into an electron-beam (EB) furnace. As the end of the wire was heated, the melted niobium formed a drop on the end of the wire. Once the size of the drop was large enough (5.49 mm to 5.54 mm in diameter), it broke away and began to fall down the tube. The size of the drop, which remains fairly constant for a set diameter of niobium wire, is determined by the liquid-to-solid surface tension and the mass of the material [1]. The particle cooled and solidified before hitting the bottom of the tube. The prototype pyrometer was set up to observe the niobium particles as they dropped down the tube.

4.3.1 Calibration

The prototype pyrometer was set up and calibrated using the blackbody calibrator

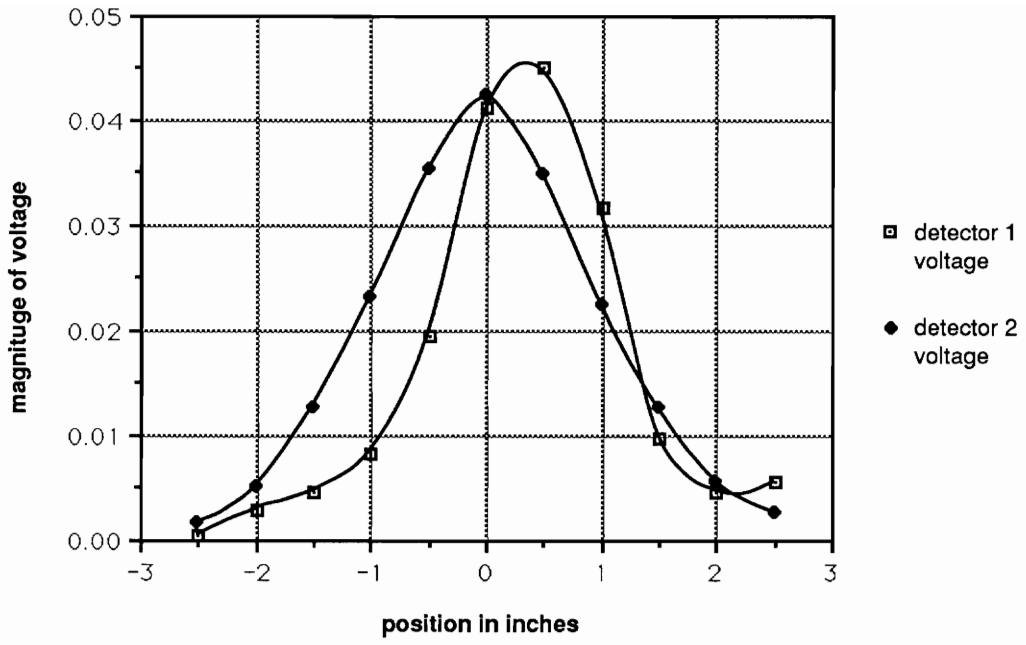

Figure 4.14. Graph of the variation in detector voltage magnitude with respect to the position of the blackbody calibrator (at 1000 °C) within the pyrometer's field-of-view.

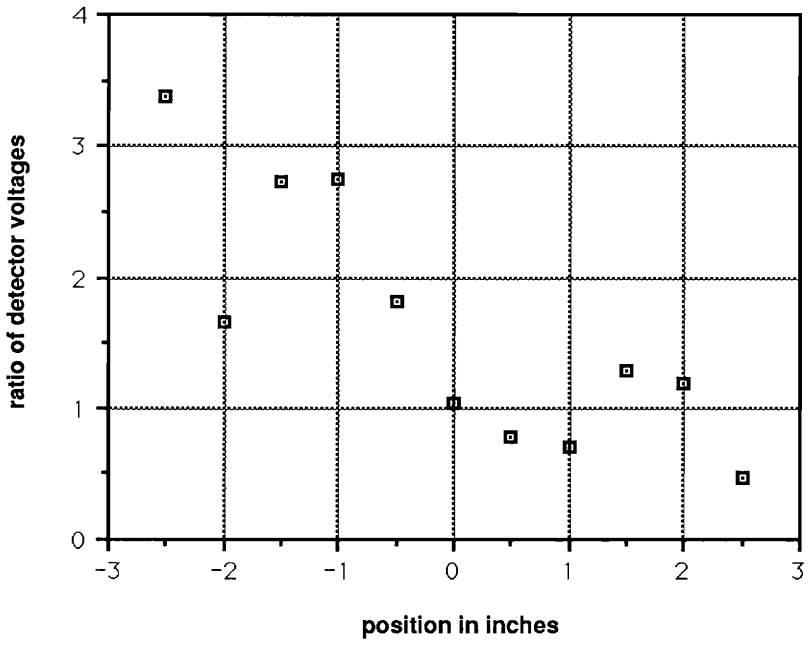

Figure 4.15. Graph of the variation in the ratio of the detector voltages with respect to the position of the blackbody calibrator (at 1000 °C) within the pyrometer's field-of-view.

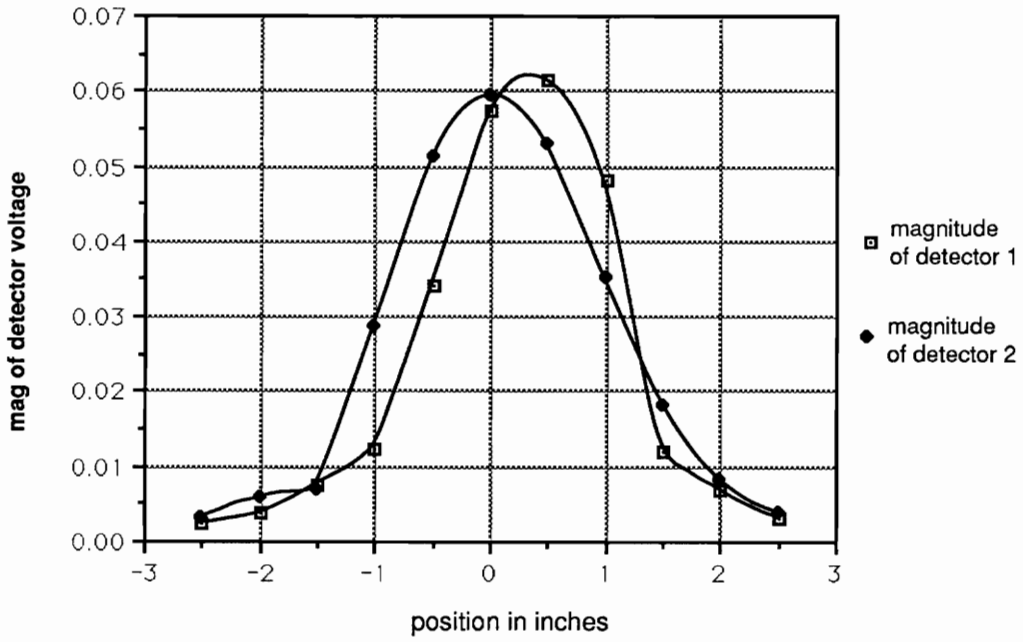

Figure 4.16. Graph of the change in detector voltages as a function of the blackbody radiator's (at 1100 °C) position within the pyrometer's field-of-view.

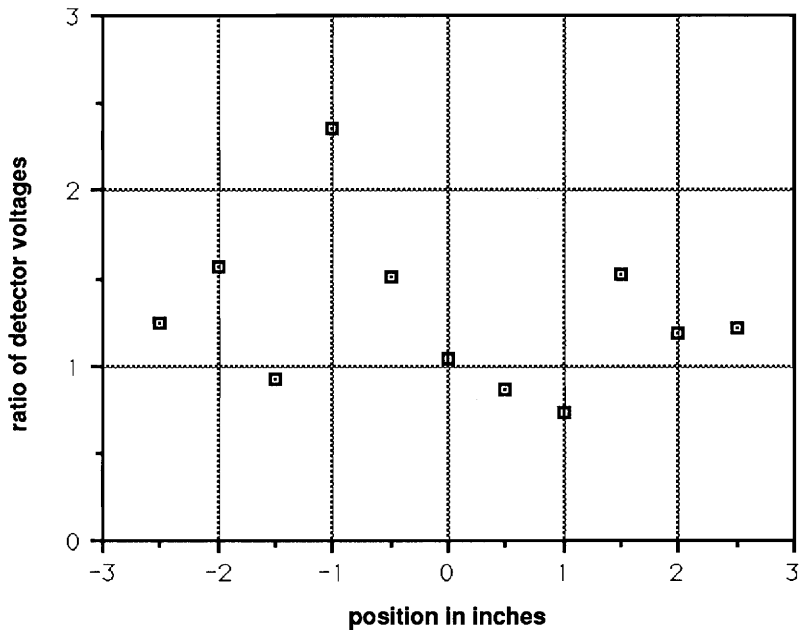

Figure 4.17. Graph of the variation in the ratio of the detector voltages with respect to the position of the blackbody calibrator (at 1100 °C) within the pyrometer's field-of-view.

as in Figure 4.9. The blackbody calibrator was set at 650°C. By monitoring the signal in both channels of the digital oscilloscope while the shutter was open, the heights of all components and angle of the beam splitter were adjusted for proper alignment. Each combination filter/lens was also moved along the track until the detectors were at the focal point of the lenses and the signal in both channels of the digital oscilloscope was optimized. After this, data was taken at four different temperatures to obtain a calibration curve for the experiments to follow. The calibration points, calculated from the data, are shown in Figure 4.18 with an exponential curve fitted to the data. Also shown is the theoretical curve for comparison.

4.3.2 Mounting Details

With all components properly mounted and aligned in the box, the pyrometer was moved to a port 22.6 meters (12^{th} level) below the EB furnace (15^{th} level). The calcium fluoride rod was carefully fed through a $2\frac{3}{4}$" Conflat vacuum flange, making sure that none of the components in the pyrometer box were bumped and knocked out of alignment. A flat-black stove pipe section previously had been inserted at the 12^{th} level port in order to decrease stray reflections from the drops on the tube. The stove pipe section was slightly skewed in the drop tube, thereby obstructing a small portion of the right side of the instrument port on the 12^{th} level.

Care was taken to minimize ground loops. The preamps of the pyrometer were attached to an instrument ground that was provided throughout the drop tube building. Once the pyrometer had been securely mounted to the tube, the drop

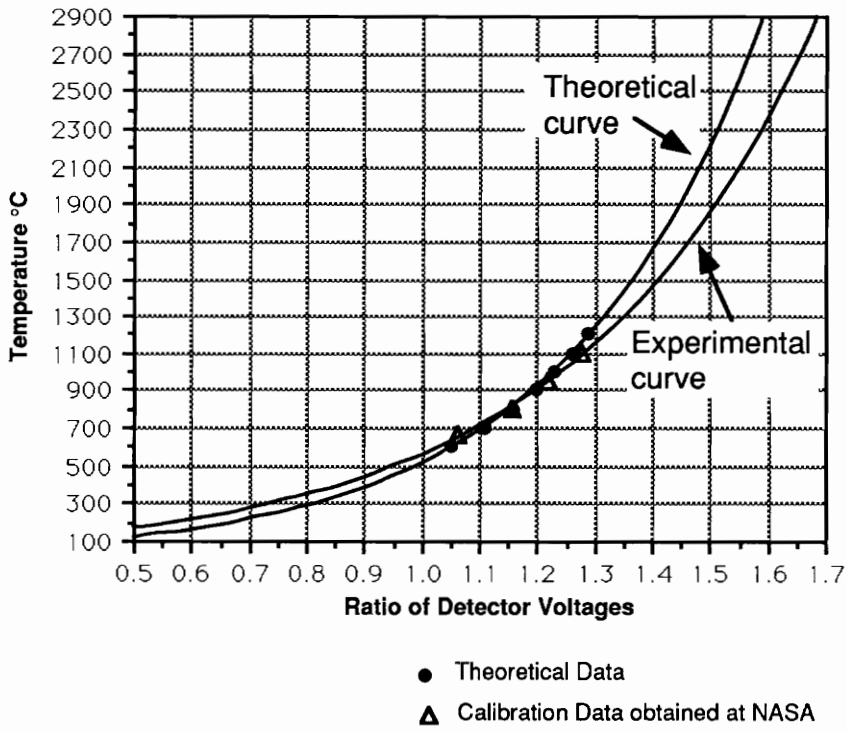

Figure 4.18. Graph of calibration curve obtained during testing of prototype pyrometer at NASA Drop Tube in Huntsville, Alabama. A theoretical curve is also shown for comparison.

tube was evacuated to approximately 10^{-6} Torr.

4.3.3 Data Acquisition

A silica photodetector, located immediately below the EB furnace, was used as a trigger for the data acquisition. The data from the detector preamps was acquired by the digital processing oscilloscope at a sampling rate of 10 kHz. A program (see Appendix D) was written in order to transfer the data from the oscilloscope to a file on the hard drive of the computer via the GPIB. Backup copies of the data files were also made on floppy disks. A plotter was used to copy the waveform obtained on the screen of the digital oscilloscope.

4.3.4 Data Analysis

4.3.4.1 Processing of Original Data

A software package called MATLAB™ was used to determine numerically the initial detector offset and the magnitude of the detector voltage from the data when the particle was detected. MATLAB™ is an interactive software package for scientific and engineering numeric computation. Figure 4.19 shows a sample of the drop data obtained from the niobium processing. MATLAB™ was used to determine the initial detector offset by having the software determine the mean value of a specific number of points before the drop event occurred. In the data in Figure 4.19, the initial offset was determined by taking the mean of points 1 through 80 on the time axis. The magnitude of the voltage when the particle was detected was determined by the same method. Due to the noise present in the signal when the particle was detected, determining the points on the time axis to be averaged was difficult. Therefore, a digital filtering technique, discussed in the

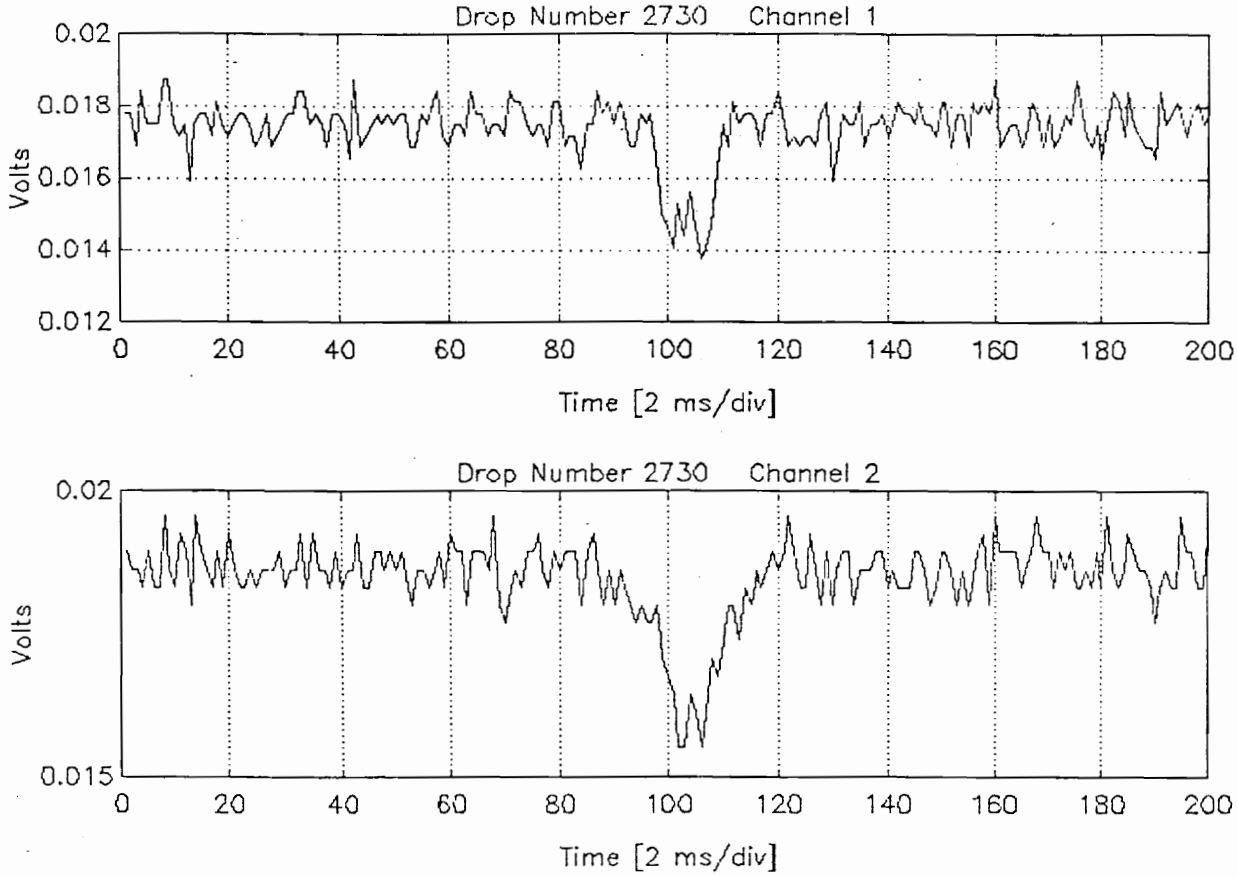

Figure 4.19 The figures show sample drop data from the niobium processing.

next section, was adopted. Table 4.1 shows the drop number and the calculated ratio of the channels for each drop detected.

4.3.4.2 Processing of Filtered Data

Due to high frequency noise present in the detector outputs, digital filtering techniques were investigated to reduce the influence of the noise. Figures 4.20 and 4.21 show the power spectral density of the noise floor for both detectors on channels 1 and 2 respectively, as calculated on MATLAB™ by a Fast Fourier Transform (FFT) routine.

Two types of low-pass digital filters were examined; these were the Butterworth filter and the Chebyshev filter. A Butterworth filter design possesses maximum flatness in the passband at the cost of less stopband attenuation. As the order, n, of the filter approaches infinity, the amplitude response of the Butterworth filter approaches an ideal lowpass filter characteristics; however, the filter delay also approaches infinity. A Chebyshev frequency-response characteristic possesses ripples within the passband while possessing the sharpest cutoff characteristics of all filters [16,17]. Different orders of the filters were looked at, as well as different cut-off frequencies. Plots of the data using cutoff frequencies from 200 Hz - 600 Hz were examined. Cut-off frequencies of 300 Hz and lower washed out the signal obtained from the niobium testing. Frequencies above 400 Hz did not significantly filter the noise within the signal. The cutoff frequency of 400 Hz was chosen because the noise component at 337 Hz, as observable in Figures 4.20 and 4.21, did not appear to effect the signal detrimentally. The Butterworth filter was chosen as the preferable filtering technique for this application over the

Drop Number	2695	2730	2734	2735	2737	2738	2745	2747	2748	2752	2753	2757	2759	2760
Ratio	2.364	1.409	1.375	1.238	1.591	1.071	1.556	2.077	1.875	1.182	0.800	1.538	1.714	0.970

Table 4.1. Shown illustrated is the drop number and the calculated ratio of the two channels using the unfiltered detector voltages for each drop detected.

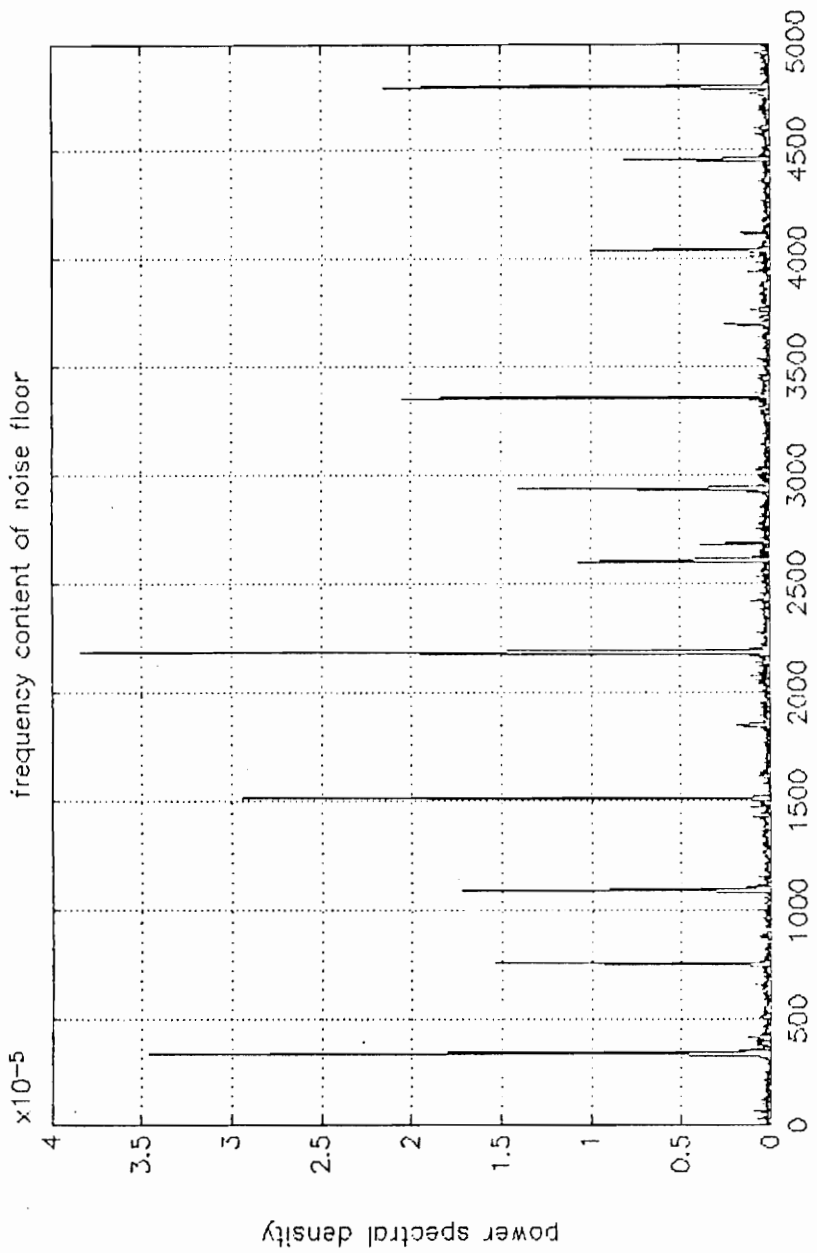

Figure 4.20. The figure shows the power spectral density of the noise floor on Channel 1.

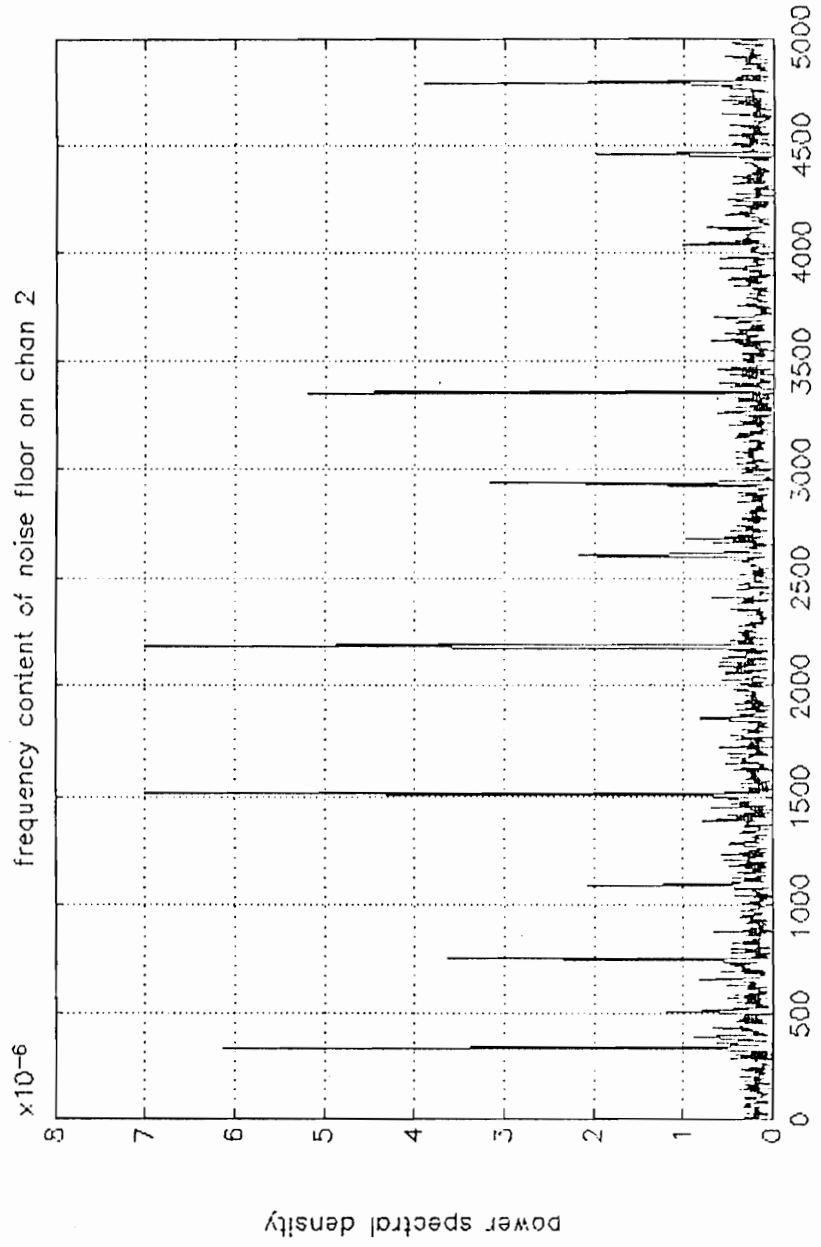

Figure 4.21. The figure shows the power spectral density of the noise floor on Channel 2.

Chebyshev due to the ripple associated with the latter. The original data was filtered with different orders (1^{st} - 4^{th}) of the Butterworth filter. MATLAB™ was again used to determine the initial detector offset and the magnitude of the voltage when the particle was detected. In Figure 4.22 the sample data from Figure 4.19 is shown filtered using a 2^{nd} order Butterworth filter with a cutoff frequency of 400 Hz. Table 4.2 shows the drop number and the ratio of the channels for each drop detected using different order filters.

4.3.5 Experimental Results

4.3.5.1 Original Data

Figure 4.23 shows the ratios of the two channels from the original data for each drop detected. For all the drops, the ratios of the unfiltered detector voltages show a standard deviation of 0.432 and a mean value of 1.483 for the ratio of the two channels. According to the calibration curve in Figure 4.18, the ratios of the drops indicate a range of temperatures from 400°C to well over 3500°C, and a mean temperature of 1800°C.

4.3.5.2 Filtered Data

Figure 4.24 shows the ratios of the two channels from the filtered data for each order of the Butterworth filter. The ratios of the filtered data show a standard deviation of 0.24 and a mean value of 1.27 for the 14 drops analyzed. The variance between the different order filters was small, as can be seen from Figure 4.24, but a different mean was obtained from that of the unfiltered data. According to the calibration curve in Figure 4.18, the ratios of the drops, excluding the outlier drop number 6 (2738), indicate a range of temperatures from

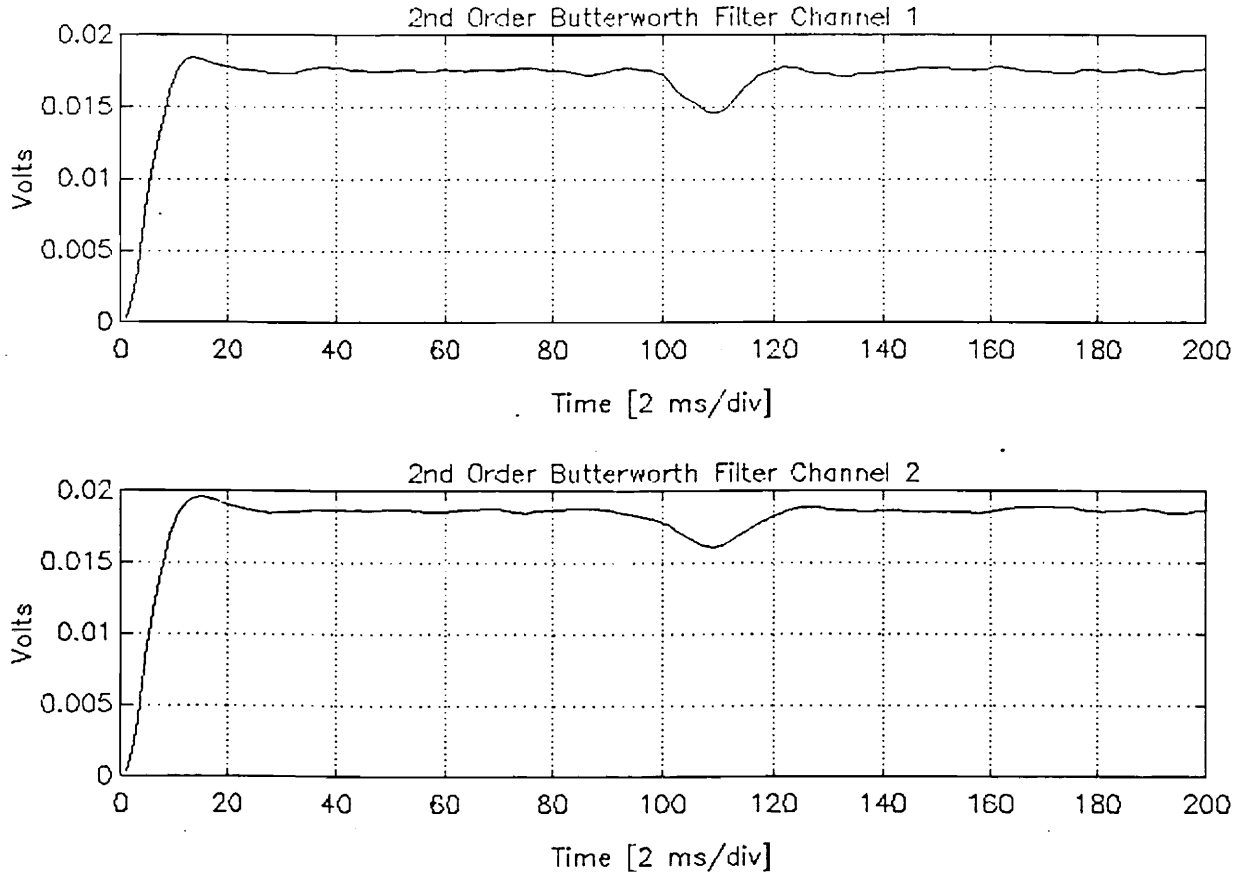

Figure 4.22. Sample data from the niobium processing is shown filtered using 2nd Order Butterworth filter.

Drop Number		2695	2730	2734	2735	2737	2738	2745	2747	2748	2752	2753	2757	2759	2760
Ratio	1st	1.500	1.160	1.300	1.143	1.240	0.562	1.333	1.667	1.462	1.172	1.133	1.200	1.318	1.226
	2nd	1.625	1.167	1.421	1.150	1.292	0.667	1.381	1.556	1.462	1.259	1.107	1.222	1.350	1.167
	3rd	1.625	1.125	1.500	1.100	1.304	0.647	1.450	1.556	1.462	1.269	1.107	1.222	1.300	1.207
	4th	1.588	1.160	1.474	1.143	1.320	0.667	1.409	1.667	1.429	1.241	1.133	1.200	1.429	1.226

Table 4.2 . Shown illustrated is the drop number and the calculated ratio of the two channels for each drop detected using different order Butterworth filters.

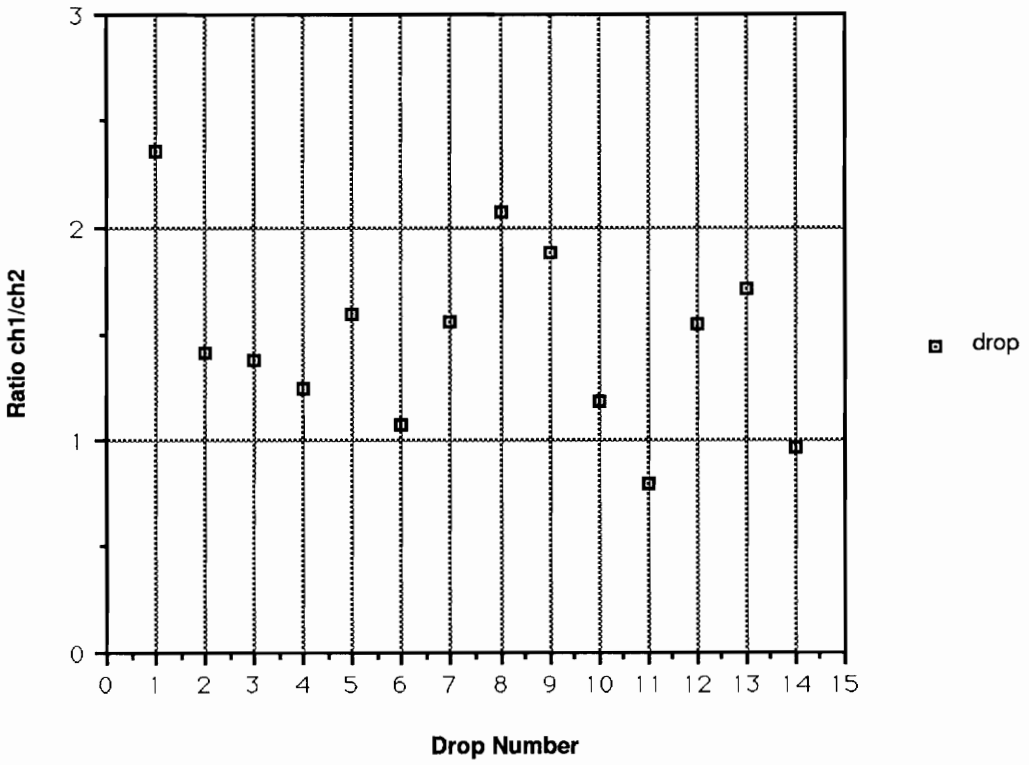

Figure 4.23. Graph of the ratios of the two channels from the original, unfiltered, detector voltages for each drop detected.

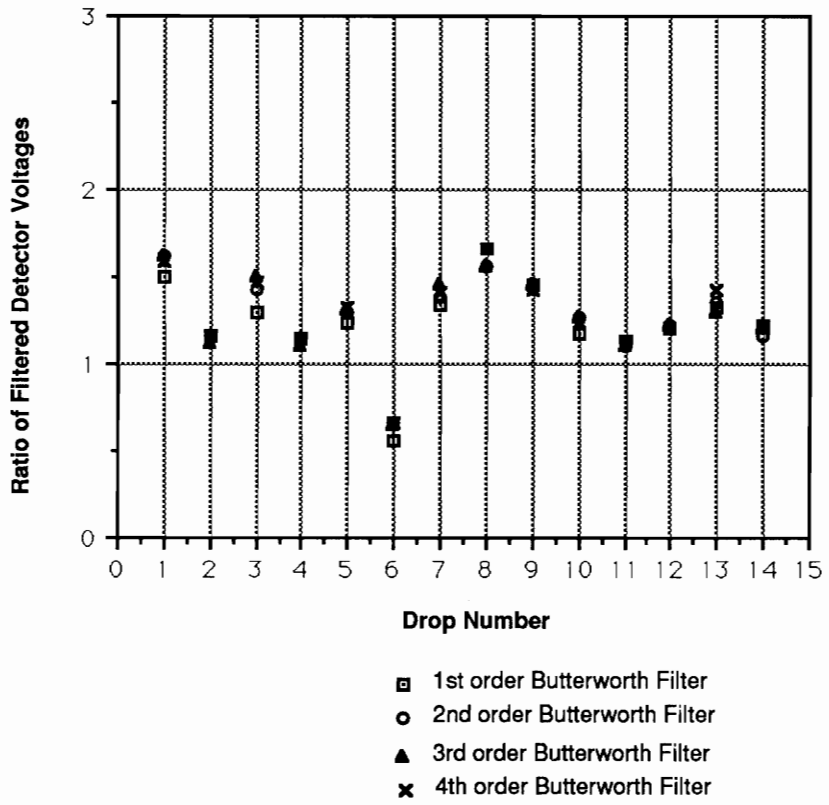

Figure 4.24. Graph of the ratios of the two channels from the filtered detector voltages for 1-4 order Butterworth digital filters.

700°C to 2300°C, and a mean temperature of 1100°C.

Because the melting point of niobium is around 2468°C, we should expect to see temperatures below that at a port 22.6 m down from the furnace [2]. This is not the case for the unfiltered data. The results from the filtered data are more realistic than those of the unfiltered data, leading to the conclusion that this is the preferred method of data analysis. In some of the drop data obtained from the field tests at NASA, data was present in only one of the two channels of the oscilloscope. The channel lacking the data was not the same each time. The oscilloscope was assumed to be working properly because former and latter drop data was observed on both channels. These interesting drops lead to the assumption that the angle of incidence of the particle radiation on the rod looking into the tube is the primary factor for the inconsistent data. The angular dependence of the pyrometer seems to be the reason for the significant variance between the drops detected at the drop tube. Since the molten particle is in free-fall, there is no way to control the position of the particle in the tube as it passes the instrument port. This may be the most serious limitation for the pyrometer in the drop tube application.

5.0 CONCLUSION

The development and testing of an optical pyrometer has been shown. The pyrometer was developed for use in a drop tube application measuring the temperature of falling molten particles as they are processed in the tube. This research effort was intended to extend experimental temperature measurement from 1100°C down to 200°C by adopting infrared transmitting components and indium antimonide photodetectors. A theoretical model was established using Planck's Law and a numerical integration routine for comparison to results obtained from laboratory calibration of the device. The use of infrared fibers and hollow core fibers and tubes was investigated for use in pyrometry, but insufficient detector power levels were obtained. With a calcium fluoride rod used as the transmission medium, laboratory testing of the pyrometer included simulating various size particles as well as observing what effect the position of the particle in the drop tube had on the pyrometer. Field testing of the pyrometer was accomplished by instrumenting the prototype on a materials processing drop tube at NASA's Marshall Space Flight Center Drop Tube Facility and taking data of niobium samples. Because of high frequency noise contributed by the detection system, a method of filtering the data with a low pass digital filter was established for aid in data analysis.

Using the digital low pass filters to smooth the data for analysis was a better approach than the unfiltered analysis because of the smaller variances between the drops and the consistency between the different orders of the filtered data. Although the variance in the filtered data was smaller than that of the unfiltered

data, estimating the temperatures with the use of the calibration curve leds to a wide range of possible temperatures. In the case of the filtered data, the range of temperatures was from 700°C to 2300°C. This wide range of possible temperature values show that the pyrometer did not operate effectively. An explanation for the poor performance of the pyrometer is probably due to the deviation of the molten particle from the center-line of the drop tube and the dependence of the pyrometer's output on the particle position. Since this particle deviation can not be controlled, possible methods to eliminate or minimize this effect can be suggested.

One option would be to work on the alignment of the components. Figures 4.14 and 4.16 show that the detector voltages with respect to position reveal relatively Gaussian curves with offset peaks. If the components could be aligned so that these peaks both correspond to the zero position, then the particle deviation problem may be overcome. Another possible option could include physically narrowing the field-of-view of the pyrometer, or more specifically, the CaF_2 rod. This may be accomplished by masking the rod so that it only sees drops which fall down the center-line of the drop tube. Another method may be to recess the rod in the flange of the drop tube instead of allowing it to penetrate into the diameter, effectively using the drop tube itself as a "blinder" for the pyrometer. Both of the latter methods would limit the use of the pyrometer, since only a few drops actually track down the center-line, but the data obtained would be more reliable and usable.

APPENDIX A: FORTRAN PROGRAM

```
C234567
*************************************************************************
This program evaluates Planck's equation at different temperatures in order to
develop data for creating blackbody radiation curves.
*************************************************************************
$LARGE
$DEBUG
      PROGRAM BBODY

      REAL*4 W(1000),R1(1000),R2(1000),R3(1000),R4(1000),C1,S(1000),
     &       L(1000),T,C2,LW(1000),LL(1000)

      OPEN(2,FILE='T650.DAT')
      OPEN(3,FILE='T1010.DAT')
      OPEN(4,FILE='T830.DAT')
      OPEN(5,FILE='T1200.DAT')
        M=300
        WRITE(2,*) M
        WRITE(3,*) M
        WRITE(4,*) M
        WRITE(5,*) M
      C1= 37413.0
      C2= 14387.9

      DO 10 I= 1,200
        W(I)= 1+FLOAT(I-1)*.1
        T= 650.0+273.0
          R1(I)= 1.0/(W(I)*T)
          R2(I)= EXP(R1(I))
          R3(I)= (C1/W(I)**5)
          R4(I)= (R2(I)**C2)
        L(I)= (R3(I)*(1.0/(R4(I)-1.0)))
        LW(I)= LOG(W(I))
        LL(I)= LOG(L(I))
        WRITE(2,100) W(I),LL(I)
        WRITE(*,*) W(I),LL(I)
 10   CONTINUE

      DO 20 I=1,200
        W(I)= 0.4+FLOAT(I-1)*0.1
        T= 1010.0+273.0
          R1(I)= 1/(W(I)*T)
          R2(I)= EXP(R1(I))
          R3(I)= (C1/W(I)**5)
          R4(I)= (R2(I)**C2)
        L(I)= (R3(I)*(1.0/(R4(I)-1.0)))
        LW(I)= LOG(W(I))
        LL(I)= LOG(L(I))
        WRITE(3,100) W(I),LL(I)
```

```
      WRITE(*,*) W(I),LL(I)
20  CONTINUE

    DO 30 I=1,200
      W(I)=1+FLOAT(I-1)*.1
      T= 830.0+273.0
        R1(I)= 1/(W(I)*T)
        R2(I)= EXP(R1(I))
        R3(I)= (C1/W(I)**5)
        R4(I)= (R2(I)**C2)
      L(I)= (R3(I)*(1.0/(R4(I)-1.0)))
      LW(I)= LOG(W(I))
      LL(I)= LOG(L(I))
      WRITE(4,100) W(I),LL(I)
      WRITE(*,*) W(I),LL(I)
30  CONTINUE

    DO 40 I=1,200
      W(I)= 0.4+FLOAT(I-1)*.1
      T= 1200.0+273.0
        R1(I)= 1/(W(I)*T)
        R2(I)= EXP(R1(I))
        R3(I)= (C1/W(I)**5)
        R4(I)= (R2(I)**C2)
      L(I)= (R3(I)*(1.0/(R4(I)-1.0)))
      LW(I)= LOG(W(I))
      LL(I)= LOG(L(I))
      WRITE(5,100) W(I),LL(I)
      WRITE(*,*) W(I),LL(I)
40  CONTINUE

100 FORMAT(2(F14.9,1X))

    STOP
    END
```

APPENDIX B: FORTRAN PROGRAM

```
C234567
**************************************************************************
This program evaluates the integral of Planck's equation over the idealized
wavelength limits of two narrowband filters, separately. It then takes the ratio of
these results to obtain a single-valued curve which is used for the ratio pyrometry
experiment.
**************************************************************************
      PROGRAM PROOF
     $DEBUG
      EXTERNAL F
      COMMON K,EMM
      INTEGER T
      REAL A1,B1,EPS,R1,E1,KF1,KE1,K,F,C1,C2,EMM,A2,B2,R2,E2,
     &     KF2,KE2,RT
      OPEN(2,FILE='PROOF.DAT')
      OPEN(3,FILE='FILTER1.DAT')
      OPEN(4,FILE='FILTER2.DAT')
      OPEN(5,FILE='RATIO.DAT')
      M=30
      WRITE(2,*)M
C  PARTICLE EMISSIVITY
      EMM=0.8
      WRITE(3,50) EMM
      WRITE(4,50) EMM
      WRITE(5,50) EMM

c  SET FILTER LIMITS
       a1=2.763
       b1=2.882
       a2=3.0465
       b2=3.1535
       EPS=0.01
      WRITE(3,150) A1,B1
      WRITE(3,151)
      WRITE(4,152) A2,B2
      WRITE(4,153)
      WRITE(5,150) A1,B1
      WRITE(5,152) A2,B2
      WRITE(5,154)
      DO 10 T=500,3500,100
        K=T+273.0
        CALL H2A1 (A1,B1,EPS,R1,E1,KF1,KE1)
        CALL H2A1 (A2,B2,EPS,R2,E2,KF2,KE2)
          WRITE (3,*) R1,T
          WRITE (4,*) R2,T
        RT=R1/R2
          WRITE(2,100) RT,T
          WRITE(5,*) RT,T
 10   CONTINUE
```

```
50   FORMAT(3X,'Particle Emissivity =',F5.4,/)
100  FORMAT(F14.9,1X,I5)
150  FORMAT(5X,'FILTER R1 where A1=',F6.3,1X,'and B1=',F6.3,
    & ' (in microns)',/)
151  FORMAT(15X,'R1',10X,'T',/)
152  FORMAT(5X,'FILTER R2 where A2=',F6.3,1X,'and B2=',F6.3,
    & ' (in microns)',/)
153  FORMAT(15X,'R2',10X,'T',/)
154  FORMAT(9X,'R1/R2',13X,'T',/)
     STOP
     END

     FUNCTION F(X)
     COMMON K,EMM
     REAL F,K,C1,C2,EMM,S1,S2,S3,S4
       C1=37413.0
       C2=14388.0
         S1=C1*EMM
         S2=EXP(1/(X*K))
         S3=(S2**C2)-1
         S4=S1/(X**5)
         F=S4/S3
     RETURN
     END
```

APPENDIX C: PYROMETER COMPONENT LIST

1 - Calcium Fluoride (CaF_2) Rod
- manufacturer: Glass Fab
- dimensions: 1" x 6" with polished endfaces

1 - Calcium Fluoride Beam Splitter
- manufacturer: Oriel Corporation
- dimensions: 1.5" in diameter

4 - Infrared Narrowband Filters
- manufacturer: Oriel Corporation
- dimensions: 1" in diameter
- center wavelength: 1.991 μm (FWHM: 66.7 nm)
- center wavelength: 2.314 μm (FWHM: 80.5 nm)
- center wavelength: 2.823 μm (FWHM: 119 nm)
- center wavelength: 3.119 μm (FWHM: 107 nm)

2 - Calcium Fluoride Lenses
- manufacturer: Ealing Electro-optics
- dimensions: 1" in diameter
- focal length: 2 inches

2 - Indium Antimonide (InSb) Photodetectors
- manufacturer: EG&G Judson
- model number: J10D Series

2 - Preamplifiers
- manufacturer: Perry Amplifier
- model number: Model 481-44

1 - Blackbody Calibrator
- manufacturer: Ircon, Inc.
- model number: Model BCH
- calibrated temperature range: 650 to 1200°C
- emittance $\geq$ 0.99
- aperture diameter: 1 inch disk about 7 inches behind the opening in the front panel

APPENDIX D: C PROGRAM

```
/* This is a C program to acquire waveforms from a LeCroy 9450 oscilloscope via
a GPIB interface. */

#include <stdio.h>
#include <math.h>
#include <stdlib.h>
#include <string.h>
#include <decl.h>

/* strdel() */
/* deletes character from string */

 void strdel(char str[], int n)
 {
   strcpy(&str[n], &str[n+1]);
 }

/* asc_convert() */
/* returns floating point values from ascii string */

 void asc_convert(char wave[], float value[])
 {
    int count2,points=0,time,num,count;
    int position;
    char temp[12];

    count = 0;
    while(count < 19000)
       {
if(wave[count] != ' ' && wave[count] != '"')
   {
    count2 = 0;
    while(wave[count] != ' '&& wave[count] != '"')
       {
   /*    printf("\n wave[%d] = %c",count,wave[count]); */
       temp[count2++] = wave[count++];
       }
    for(position = count2; position<11; position++)
       {
       strdel(temp,count2);
       }
    value[points] = atof(temp);
 /*   printf("\ntemp = %s\n",temp);
    printf("\nvalue[%d] = %f\n",points,value[points]); */
    points++;
   }
else
   count++;
       }
```

```
}
main()
{
 char command1[70],command2[70],command3[70],command4[70],command5[70];
 char command6[70],command7[70],command8[70],command9[70],comm10[70];
 char comm11[70],comm12[70],comm13[70],comm14[70],comm15[70],comm16[70];
 int lec, board, start, count=0, i;
 char wave[21000];
 char pc[ ] = "GPIB0";
 char device5[ ] = "DEV5";
 float value[1500];
 FILE *fp1, *fp2;

 if ((board = ibfind (pc)) < 0) printf(" can't find board\n");
 if ((lec = ibfind (device5)) < 0) printf(" can't find device\n");
 if( (fp1 = fopen( "rod1.dat","w" )) != NULL )
 if( (fp2 = fopen( "rod2.dat","w" )) != NULL )

/* Create useful strings for communicating with the LeCroy */
 #define command1 "GRID DUAL"
 #define command2 "TDIV .5S"
 #define command3 "C1:VDIV 20MV"
 #define command4 "C2:VDIV 20MV"
 #define command5 "C1:TRSL NEG"
 #define command6 "TRMD SINGLE"
 #define command7 "TRDL .5S"
 #define command8 "CHDR OFF"
 #define command9 "C2:TRCP DC"
 #define comm10 "C1:CPL D50"
 #define comm11 "C2:CPL D50"
 #define comm12 "C1:INSP? 'SIMPLE',FLOAT"
 #define comm13 "C2:INSP? 'SIMPLE',FLOAT"
 #define comm14 "WFSU SP,0,NP,1500,FP,4050"
 #define comm15 "CMFT DEF9,BYTE,BIN"

/* ibclr(lec); */
 ibwrt(lec,command1,9);
 ibwrt(lec,command2,8);
 ibwrt(lec,command3,12);
 ibwrt(lec,command4,12);
 ibwrt(lec,command5,11);
 ibwrt(lec,command6,11);
 ibwrt(lec,command7,8);
 ibwrt(lec,command8,8);
 ibwrt(lec,command9,10);
 ibwrt(lec,comm10,10);
 ibwrt(lec,comm11,10);
 ibwrt(lec,comm14,22);
 ibwrt(lec,comm15,18);

 ibwrt(lec,comm12,23);
```

```
ibrd(lec,wave,20000);
printf("\n FILTER1 DATA = %s\n",wave);
asc_convert(wave,value);

for( i=0; i<1425; i++)
   fprintf( fp1, "\n%f", value[i]);
fclose( fp1 );

ibwrt(lec,comm13,23);
ibrd(lec,wave,20000);
printf("\n FILTER2 DATA = %s\n",wave);
asc_convert(wave,value);

for( i=0; i<1425; i++)
   fprintf( fp2, "\n%f", value[i]);
fclose( fp2 );

ibclr(lec);
ibsic(board);
ibsre(board,0);
ibsic(board);
}
```

REFERENCES

1. Rathz, T.J., Robinson, M.B., "The NASA/Marshall Space Flight Center Drop Tube User's Manual," NASA TM-100392, 1990.

2. Robinson, M.B., "Radiative Gas Cooling of Falling Molten Drops," NASA TM-78189, 1978.

3. Hofmeister, W., Bayuzick, R.J., "Non-contact Temperature Measurement of a Falling Drop," Center for the Space Processing of Engineering Materials, Vanderbilt University, Tennessee, 1988.

4. Corion Product Literature, "Optical Filters and Coatings," Corion Corporation, MA., 1986.

5. Kuhn, T.S., Blackbody Theory and the Quantum Discontinuity 1894 - 1912, Clarendon Press, Oxford University Press, New York, 1978.

6. Kangro, H., Early History of Planck's Radiation Law, Taylor & Francis Ltd., London, 1976.

7. Doeblin, E.O., Measurement Systems, Application and Design, McGraw-Hill Book Company, New York, 1983.

8. Levi, L., Handbook of Tables of Function for Applied Optics, CRC Press, Inc., Ohio, 1974.

9. Wyatt, C.L., Radiametric System Design, Macmillan Publishing Co., New York, 1987.

10. Jorgenson, F.R.A., Zuiderwyk, M., "Two - colour pyrometer measurement of the temperature of individual combusting particles," J. Phys. E: Sci. Instrum., Vol. 18, 486, 1985.

11. Milton, J.S., Arnold, J.C., Probability and Statistics in the Engineering and Computing Sciences, McGraw-Hill, Inc., New York, 1986.

12. Walpole, R.E., Myers, R.H., Probability and Statistics for Engineers and Scientists, Macmillan Publishing Co., New York, 1989.

13. Bornstein, A., Bichman, P. "Multimode and single-mode IR fiber characterization," Proceedings of SPIE, Vol. 1048, Infrared Fiber Optics, CA., 1989.

14. Harrington, J.A., Gregory, C.C., Nubling, R.K., "Hollow waveguides for CO_2 delivery systems," Proceedings of SPIE, Vol. 1048, Infrared Fiber Optics, CA., 1989.

15. Dror, J., Gannot, I., Croitoru, N.I., "Hollow tubes for transmitting IR laser energy for surgery applications," Proceedings of SPIE, Vol. 1048, Infrared Fiber Optics, CA., 1989.

14. Milman, J., Microelectronics, McGraw-Hill Book Company, New York, 1979.

15. Ziemer, R.E., Tranter, W.H., Principles of Communications - Systems, Modulation, and Noise, Houghton Mifflin Company, 1976.

VITA

Sara Elizabeth Moneyhun was born in Cheyenne, Wyoming, on the morning of December 15, 1964. The morning temperature was -44°F, and the high for that day was a toasty -16°F. She has yet to recover from the the chill; that is why summer is her favorite season. In 1988, she graduated from Virginia Tech with a B.S. in Electrical Engineering, whereupon she decided to pursue a Master's degree and specialize in the area of fiber optics. In her free time, Sara is inspired by her hero, Louis Comfort Tiffany, into creating intricate stained glass windows and lampshades.